Reply to reviewer #1

We are grateful for the helpful comments on the submitted version of the manuscript. Our point-by-point replies are shown in italic font.

We have edited and rewritten much of the paper to improve the use of English and also to improve the clarity of the scientific content.

Reviewer 1:
Review of *amt*2017463, Dorrestijn et al.

GENERAL
The entire abstract will need to be rewritten in view of the results contained in the DOIs listed at the end of this review. It reflects omissions and mistaken assumptions listed in the detailed commentary that follows. The scaling of variance has to recognise that the variance of atmospheric variables obtained by observations acquired by adequate measurement techniques does not converge. That is one of several relevant results obtained by the finding that atmospheric variables have non-Gaussian probability distributions, with fat-tailed power laws best represented by Lévy statistics. The zoo of scaling behaviours displayed in this manuscript arises from this basic fact and its consequences. These facts have to be at least recognised as being in existence rather than simply ignored as in the present manuscript.

We thank the reviewer for this important perspective. After careful consideration of the material referenced in the DOIs, the authors fully agree with this assessment and furthermore have had an opportunity to identify appropriate modifications to the manuscript that we hope satisfactorily address the reviewer comments.

First, we acknowledge that the relevance of non-Gaussian distributions of temperature and specific humidity has indeed been addressed insufficiently in the submitted manuscript. We have added text and references to the manuscript and have added a statement reflecting this fact in the abstract. Second, we also acknowledge that the same holds true for the effects of 3D anisotropy and vertical scaling that can alias into horizontal variance scaling exponents on isobaric surfaces. The scale breaks may indeed be partly a result of the effects of vertical scaling. Therefore, we have rewritten the abstract and the entire manuscript and now reference the suggested DOI's.

Here is the new version of the abstract:

Satellite observations are used to obtain vertical profiles of variance scaling of temperature (T) and specific humidity (q) in the atmosphere. A higher spatial resolution retrieval at 13.5 km complements previous Atmospheric Infrared Sounder (AIRS) investigations with 45 km resolution retrievals and enables the derivation of power law scaling exponents to length scales as small as 55 km. We introduce a variable-sized circular-area Monte Carlo methodology to compute exponents instantaneously within the swath of AIRS that yields additional insight into scaling behavior. While this method is approximate and some biases are likely to exist within non-Gaussian portions of the satellite observational swaths of T and q, this method enables the estimation of scale-dependent behavior within instantaneous swaths for individual tropical and extratropical systems of interest. Scaling exponents are shown to fluctuate between β = -1 and -3 at scales $\geq$500 km, while at scales $\leq$500 km they are typically near $\beta \approx$ -2, with q slightly lower than T at the smallest scales observed. In the extratropics, the large-scale β is near -3. Within the tropics, however, the large-scale β for T is closer to -1 as small-scale moist convective processes dominate. In the tropics, q exhibits large-scale β between -2 and -3. The values of β are generally consistent with previous works of either time-averaged spatial variance estimates, or aircraft

observations that require averaging over numerous flight observational segments. The instantaneous variance scaling methodology is relevant for cloud parameterization development and the assessment of time variability of scaling exponents.

The following modifications to the manuscript refer to the references in the list of DOIs:

Starting on Page 11, line 19: "The large variety of exponents is likely due to some extent from the turbulent structure of T and q fields with long-tailed non-Gaussian distributions (Tuck, 2010). These behaviors may inhibit the precise estimation of variance scaling exponents from observations. Further research is necessary to determine the impacts of the non-Gaussian distribution shapes of T and q on derived exponents, and their scale- dependence of non-Gaussianity. This effect may contribute to spreading out the PDFs of exponents."

Starting on Page 10, line 25: "Lovejoy et al. (2009) and Pinel et al. (2012) showed that scale-breaks detected by in situ aircraft observations may be the result of 3D anisotropy in atmospheric properties. In Pinel et al. (2012), scale breaks are observed in the 100 - 500 km range with horizontal exponents that transition from -5/3 to -2.4. In the vertical direction, an exponent of -2.4 is derived and suggests that gently sloping isobaric aircraft trajectories are the source of the transition to -2.4. Since the T and q exponents reside on isobaric surfaces (e.g. 500 hPa) in this work, one may expect that the vertical exponents may alias into the large-scale horizontal exponents. However, we do not find a clear indication of $\beta_L = -2.4$, although a focused effort on obtaining vertical scaling exponents with satellite soundings warrants further investigation. Unfortunately, the relative coarse vertical resolution of ~ 2 km from AIRS retrievals is not ideal for obtaining reliable estimates of vertical scaling exponents; dropsondes and radiosondes remain the standard and are much better suited to this observational challenge."

DETAILED COMMENTARY

Page 1, Lines 16-18: Energy is deposited in the atmosphere by the absorption of photons by molecules, that is to say it has no alternative but to propagate upscale. This is argued at length in some of the references supplied as DOIs.

We now refer to Tuck (2010) in which upscale energy propagation is discussed. We have added the following on Page 1, line 21: "a review paper on upscale energy propagation is found in Tuck (2010)."

Lines 18 et seq: See the last, 8th, DOI for a refutation of these arguments. They are profoundly mistaken.

We mention upscale energy transfer in 2D and quasi-geostrophic turbulence starting on page 1 line 18. In the 8th DOI (Schertzer et al. 2012) "Quasi-geostrophic turbulence and generalized scale invariance, a theoretical reply" give an alternative theory of energy transfer using fractal dimension turbulence. We add to the manuscript starting on page 1 and line 20: "Schertzer et al. (2012) give an alternative theory of energy transfer using fractal dimension turbulence."

Page 2, Lines 3-14: Inspection of the DOIs supplied will show a view differing substantially from that in these references. The Lindborg papers especially rest on bad assumptions. The Lovejoy & Schertzer book also has a lot on scaling in models, an advance on lines 15-28.

Although the reviewer suggests that the Lindborg paper may rest on bad assumptions, we mention the Lindborg paper because it reproduces the Nastrom and Gage figure to bolster its well-known results from aircraft data.

Section 3: KT09 in my opinion deploys flawed analytical methods. If the authors insist on using it, it must be justified in the light of the conclusions reached in the DOIs below. That includes the results on how easy it is to find false scale breaks, especially if less than three decades of good quality observations are present. They cannot be simply ignored.

First, we refer to the two additional revised blocks of text and references added above starting on Page 11 and line 19, and Page 10 and line 25.

Second, given the limitations stated above, the "poor man's spectral analysis" does have some advantages in particular for data sets as described in this manuscript that do not span three decades of scales. We address them in the short paragraph starting on Page 11 and line 11. "A major advantage of the "poor man's spectral analysis" method (Lorenz, 1979) is that relatively small datasets are sufficient to estimate variance scaling exponents. Reliable spectral power diagrams of observational data arise only after averaging over relatively large datasets. For instance, Nastrom and Gage (1985) obtained their spectral power diagrams by averaging over observations collected during 6,000 commercial aircraft flights. The calculation of spatial variances is still possible in the event of missing or poor quality data, in which case conventional spectral analysis cannot be employed (Vogelzang et al., 2015)"

Third, the reviewer is right in that we need clearer justification for using this methodology. In the abstract we have now made clearer that we need instantaneous estimates of the scale-dependent variance: "... this method enables the estimation of scale-dependent behavior within instantaneous swaths for individual tropical and extratropical systems of interest."

Furthermore, we have enhanced the discussion at the end of the paper on why the authors think this approach is meritorious, despite its limitations and need for further investigation. At this time, we are not aware of any other approaches that can be used to exploit satellite soundings of T and q to quantify individual storm evolution and structure of scaling exponents, which are inherently tied to their predictability. We have significantly added to and revised the last paragraph starting on Page 12 and line 5:
"This novel instantaneous variance scaling methodology may enable detailed examination of the variance scaling of the time evolution of storm systems, such as extratropical cyclones at different stages in their lifecycle as previously demonstrated with numerical simulations by Waite and Snyder (2013), or with deep convection along the Mei-Yu front by Peng et al. (2014). The changes in the kinetic energy spectra in Waite and Snyder (2013) and Peng et al. (2014) occur on time scales of hours to several days. We postulate that scaling exponents derived from instantaneous snapshots obtained from satellite swath data will be useful observational constraints for time-dependent spectra generated from numerical modeling experiments. To conclude, it is well known that the time scale of predictability is closely linked to the spatial scale of the phenomenon of interest (Lorenz, 1969). In the case of moist baroclinic waves, steeper (shallower) spectral slopes at small scales for individual baroclinic waves are inherently more (less) predictable as the slope portrays the relative importance of convection within any given disturbance (Zhang et al., 2007). As a result, the instantaneous scaling exponents are expected to potentially offer a new type of observational constraint with relevance to the predictability of individual tropical or extratropical disturbances."

Sections 4 and 5: At the very least these will have to be rewritten to accommodate the existence of alternative

views and results conatined in the DOIs and books listed below. For example, models contain assumptions about variances and covariances being random that are at odds with observed reality; that is one of many problems.

We hope that the revisions and responses described above generally address these concerns. We have rewritten much of the paper to improve clarity of content and have added and revised many paragraphs taking into account the suggested DOIs (which were very helpful). The reviewer comment above regarding models (we assume numerical) is well taken. There are numerous issues of interest in numerical models, but those aspects are well beyond the scope of this article. We hope to advance this methodology on evaluating numerical model output in the near future, however.

Reply to reviewer #2

We are grateful for the helpful comments on the submitted version of the manuscript. Our point-by- point replies are shown in italic font.

We have edited and rewritten much of the paper to improve the use of English and also to improve the clarity of the scientific content.

Reviewer 2:
Review of *amt*2017463, Dorrestijn et al.
Atmos. Meas. Tech. Discuss., doi:10.5194/amt-2017-463-RC2, 2018 Interactive comment on Instantaneous variance scaling of AIRS profiles using a circular area Monte Carlo approach by Jesse Dorrestijn et al. Anonymous Referee #2
Received and published: 6 February 2018

Overall / general comments
The paper presents a circular area Monte Carlo approach to assess scale invariance properties and scale breaks from AIRS measurements. Overall the paper is very well written but the statistics and correlations showed here are not always convincing. This is a promising technique but it needs to be apply to more data and to acknowledge the poor correlations observed in section 4.5 (and more data will help with correlations). Also, why sometime the authors use /alpha and sometime β? Is generally more known, especially when its concerns the well-known -5/3 value. There is no such reference for /alpha. I suggest using through the whole manuscript for consistency reasons.

We agree that the datasets used for the correlation analysis are small. As this manuscript is meant to be a methodology rather than a full exploration of the potential of AIRS data, the computational expense of calculating the exponents is large, and the single infrared field of view retrieval of Irion et al. (2018) has not yet been operationalized, we are unable to go much further with more robust statistics in this initial study. In response to the reviewer comment, we have removed the three panels with the smallest correlation coefficients from Fig. 10. We argue that the six panels with the largest correlation coefficients are sufficiently large that, in our opinion, add value to the paper. We acknowledge that the usage of α and β values could be somewhat confusing at times. Despite this, we choose to include them both in the new manuscript because many of the referenced studies use both types of exponents. The left and right axes on Figures 5–8 are intended to help guide the reader between these two exponents. The variance scaling exponents that we calculate are actually α values, also used by KT09, therefore we choose to show them. Omitting the β values would devalue the paper, since these are better known.

We have added the following to the manuscript starting on Page 8 and line 33: "...the sample size from the limited set of granules is unable to yield a robust histogram. Our intent is to instead demonstrate the new scaling approach. A much larger and statistically robust dataset is outside the scope of this work."

Minor comments: Abstract Line 2: 13.5km is not really what I call high spatial resolution. May be higher is better for the comparison with 45 km.

We agree and use the word "higher".

Introduction: Line 18: Please add also the reference: Kolmogorov, A. N.: Dissipation of Energy in the Locally Isotropic Turbulence, Proceedings of the USSR Academy of Sciences (Russian), translated into English by Kolmogorov, Andrey Nikolaevich (8 July 1991), 23, 16 18, 1941.

Thanks. We now include this reference.

2.2 Line 9: Why Retrieval System have their first letter in capital?

This was a mistake. It should indeed be lowercase.

Figure 3: Please increase text/label font size It would be interesting to highlight (using arrow, line, marker, etc) the position of the scale break for each case. It would be more easy for the reader to see if there is a common off-set between the AIRS-xxx in the 4 locations.

We agree and changed the sizes. Scale breaks are introduced later in the paper and we think it would be too much information for the reader to digest if we put them into these figures before they are explained.

Figure 4c: The large decreasing of standard deviation as a function of the length scale in the case AIRS-OE need to be more developed. This slope catches the eye directly when looking at the figure. This is probably due to small scale processes that are resolved with the higher resolutions but it should be mentioned.

We agree this needs some additional description, and we added a comment to the manuscript starting on Page 7 and line 10: "In Fig. 4c, the discrepancies between the four retrievals are more significant at larger l, where AIRS-OE shows a decreasing standard deviation as a function of increasing l. However, the AIRS-OE with a peak around 8° may be a result of finer-scale fluctuations that are only captured by AIRS-OE."

4.5 Line 13: To me well-correlated is above 0.80, we can argue that the fig 10a is close to this value but then the correlation decrease. It becomes dangerous to me to talk about correlation below 0.7. This is especially true for water vapor where the values are too low. I can be simpler to remove WV from this plot and keep temperature only.

Per the earlier comments above, we removed the three panels with the lowest correlations from figure 10. We believe that the six panels shown in the figure adds additional value to the paper."

Interactive comment on Atmos. Meas. Tech. Discuss., doi:10.5194/amt-2017-463, 2018.

Instantaneous variance scaling of AIRS thermodynamic profiles using a circular area Monte Carlo approach

Jesse Dorrestijn, Brian H. Kahn, João Teixeira, and Fredrick W. Irion

Jet Propulsion Laboratory, California Institute of Technology, 4800 Oak Grove Drive, Pasadena, CA 91109, USA

Correspondence: Brian H. Kahn (brian.h.kahn@jpl.nasa.gov)

Abstract. Satellite observations are used to ~~study~~ obtain vertical profiles of ~~the~~ variance scaling of temperature (T) and ~~water vapor~~ specific humidity (q) in the atmosphere. A higher spatial resolution retrieval at ~~of~~ 13.5 km ~~at nadir, instead of 45 km as in~~ complements previous Atmospheric Infrared Sounder (AIRS) ~~studies~~ investigations with 45 km resolution retrievals and enables the derivation of ~~the variance-scaling~~ power law scaling exponents ~~down~~ to length scales ~~of~~ as small as 55 km. ~~With~~ ~~the~~ We introduce a variable-size circular-area Monte Carlo ~~approach~~ methodology to compute~~the~~ exponents ~~can be computed~~ instantaneously ~~along the track of Aqua,~~ within the swath of AIRS ~~which gives more~~ that yields additional insight into ~~the~~ scaling behavior. ~~of the atmospheric variables in individual Level 2 satellite granules~~ While this method is approximate and some biases are likely to exist within non-Gaussian portions of the satellite observational swaths of T and q, this method enables the estimation of scale-dependent behavior within instantaneous swaths for individual tropical and extratropical systems of interest. Scaling exponents are shown to fluctuate heavily between $\beta = -1$ and ~~$\beta =$~~ -3 at ~~the larger~~ scales $\geq$ 500 km, while at ~~the smaller~~ scales $\leq$ 500 km they are ~~often~~ typically~~closer to~~ near $\beta = -2$, ~~and they decrease a bit for moisture~~ with q slightly lower than T at the smallest scales ~~that are considered~~ observed. ~~Outside the tropics~~ In the extratropics, the ~~temperature~~ large-scale ~~variance-scaling exponent~~β is ~~often close to~~ near -3 ~~due to large temperature slopes that are present along the track of Aqua likely as a result of geostrophic turbulence~~. ~~Around~~ Within the tropics, however , ~~this exponent~~ the large-scale β for T is ~~often~~ closer to -1 ~~,because the tropical atmosphere is dominated by smaller-scale processes such as moist convection~~ as small-scale moist convective processes dominate.~~, leading to an observable reverse scale break. In contrast, water vapor is shown to have large-scale exponents often close to -3 around the tropics, because there, large-scale water vapor slopes are common along the Aqua track.~~ In the tropics, q exhibits large-scale β between -2 and -3. The values of β are generally consistent with previous works of either time-averaged spatial variance estimates, or aircraft observations that require averaging over numerous flight observational segments.~~Furthermore, the scale-break length scale turns out to be highly variable and shows a large spread. The presented variance-scaling results are of importance~~ The instantaneous variance scaling methodology is relevant for cloud parameterization ~~purposes~~ development and the assessment of time variability of scaling exponents.

1 Introduction

~~The atmosphere distributes its kinetic and thermal energy over its entire range of scales.~~ In the atmosphere, energy that is present at larger scales tends to cascade towards the smaller scales where kinetic energy is turned into heat by dissipation at the Kolmogorov length scale (Hunt and Vassilicos, 1991); Kolmogorov, 1991). ~~A complicating factor is that Earth's atmosphere as a whole is near two-dimensional, while at the smaller scales it is three-dimensional~~. In two-dimensional turbulence, or quasi-geostrophic turbulence, ~~enstrophy is conserved (Kraichnan, 1967;Leith, 1968) such that~~ energy that is injected at the smaller scales can also be transferred ~~towards the~~to larger scales (Lindborg, 1999; Charney, 1971; Fjørtoft, 1953). Schertzer et al. (2012) give an alternative theory of energy transfer using fractal dimension turbulence. A review on upscale energy propagation is found in Tuck (2010). ~~Furthermore, n~~Numerous processes affect the atmosphere at different length scales (e.g. the large-scale planetary circulation, synoptic-scale systems, ~~clouds,~~ organized and isolated deep convection, shallow convection, turbulence, and molecular diffusion). ~~Therefore~~ As a result, the rate at which the variance of atmospheric ~~variables~~ properties changes as a function of length scale, the *variance scaling*, is not uniform over the entire range of scales of Earth's atmosphere.

Observations have been frequently used to demonstrate that atmospheric variables satisfy specific scaling laws. Julian et al. (1970) showed that at ~~the~~ larger scales ($>$ 1,500 km) the kinetic energy spectra ~~tend to be close to~~ follow a k^{-3} law. At smaller scales ($<$ 500 - 700 km) the ~~slope of the~~ spectra ~~is~~ are shallower and ~~prefers~~ follow more closely a $k^{-5/3}$ law. ~~, which t~~Transitions in between these regimes ~~has~~ have been clearly demonstrated with aircraft observations of wind and temperature by Nastrom and Gage (1985). ~~Their variance power spectra diagram~~ The Nastrom and Gage (1985) variance power spectra diagram (their Fig. 3 ~~of Nastrom and Gage (1985)~~) ~~has~~ is often ~~been~~ cited and reproduced (e.g. Lindborg (1999); Tung and Orlando (2003); Palmer (2012)). The precise variance scaling exponents of these atmospheric variables ~~is~~ are, however, more complicated and subtle. For instance, exponents that transition from $-5/3$ to -2.4 between 100 km and 500 km ~~have been found~~ were observed in aircraft wind measurements by Pinel et al. (2012).

Kahn and Teixeira (2009) (KT09 hereafter) ~~have~~ used satellite observations of temperature (T) and ~~water vapor~~ specific humidity (q) to derive sensitivities of scaling exponents to ~~several~~ multiple factors such as the location on Earth (land, ocean, latitude), the season, and the ~~presence~~ existence of clouds or clear sky. ~~and surface conditions (land or ocean).~~ The underlying causes of these ~~sensitivities~~ variations and ~~even~~ more ~~complicated~~ complex phenomena such as scale breaks and reverse scale breaks (demonstrated to exist by KT09), are not yet fully understood. One of the reasons ~~is~~ may be the paucity of extensive observational data sets that ~~corresponding~~ correspond to well-defined atmospheric conditions ~~for a large range of scales~~ over several orders of length scales. ~~Furthermore, c~~Clear ~~sensitivities~~ patterns of scaling exponents ~~in an area~~ only appear ~~only~~ after averaging over a sufficient time period~~s~~ on the order of a season (KT09).

A myriad of ~~studies~~ investigations using ~~of~~ atmospheric variability generated by ~~with~~ numerical models have been performed. ~~, e.g.~~ Jonker et al. (1999) used a large-eddy simulation (LES) model to show that passive scalars in a turbulent field ~~can possess~~ exhibit different power spectra than the thermodynamic variables themselves. Cusack et al. (1999) ~~studied~~ used the horizontal variance of moisture with global weather model analysis data and constructed a cloud parameterization from it.

Hamilton et al. (2008) showed ~~the~~ a transition from a steep k^{-3} law to a shallower $k^{-5/3}$ law in the kinetic energy spectrum of a general circulation model (GCM).

~~Just a~~As with observations, numerical simulations have their ~~restrictions~~ own limitations considering the range of scales that ~~they cover~~ are represented.~~: d~~ Due to computational restrictions, LES models ~~can not yet~~ are not able to accurately simulate synoptic systems. ~~, while on the other hand~~ GCMs and cloud resolving models (CRMs) are not able to accurately ~~do not~~ resolve smaller-scale processes (e.g. turbulence, shallow convection) that affect ~~the~~ variance scaling exponents at all scales. Parameterizations of ~~these~~ unresolved processes are ~~often~~ based on assumptions about variance scaling exponents derived from larger scales (Bogenschutz and Krueger, 2013; Tompkins, 2002; Teixeira and Hogan, 2002; Larson et al., 2002), and therefore, can not be used to ~~derive~~ infer independent estimates of variance scaling exponents ~~at or close to~~ near the subgrid-scales. In short, there ~~is~~ remains a need for numerical and observational ~~studies~~ investigations that ~~deliver~~ report statistics of ~~the~~ scaling exponents ~~at an increased~~ over a larger range of length scales, in particular near the GCM subgrid-scale (Kahn et al., 2011). In Lovejoy and Schertzer (2013) one can find more about scaling in models.

In a ~~To~~ follow-up ~~on~~ to the ~~work~~ methodology described by KT09, this ~~paper~~ work presents a new variance scaling method ~~which~~ that is applied to vertically resolved, satellite ~~data~~ derived ~~atmospheric temperature~~ T and ~~water vapor mass mixing ratio~~ q with a higher horizontal resolution ~~(three times higher in both horizontal directions)~~ than previously reported . The new variance scaling method enables the calculation of instantaneous variance scaling exponents along the ~~track~~ swath of Earth observing satellites. For a ~~given~~ particular horizontal two-dimensional atmospheric field (e.g. ~~temperature, water vapor~~ T or q) at a ~~certain~~ particular pressure level or altitude in the atmosphere, standard deviations are calculated over spatial areas for a range of length scales from which variance scaling exponents are derived. Areas are chosen to be of *circular* shape and ~~can be~~ are placed along the track of a satellite. Variance ~~scaling exponents~~ spectra are ~~estimated~~ derived by varying the diameter of the circular areas. Then exponents are derived by fitting power law exponents to the data. To ~~get~~ obtain ~~adequate~~ robust estimates, a Monte Carlo method is employed~~, which uses~~ that randomly place~~d~~s smaller circles ~~inside~~ within ~~a large~~ the largest diameter circle.

The paper is organized as follows: Section 2 describes the ~~atmospheric~~ temperature and specific humidity datasets, which is followed by ~~a section that introduces~~ the introduction of the new variance-scaling method (Section 3). The variance scaling results are presented in Section 4. ~~Finally~~ Lastly, Section 5 discusses the implications and conclusions of the main findings, ~~draws conclusions and presents~~ and suggests future ~~work~~ research that is ~~possible~~ enabled with this ~~newly developed~~ novel approach.

2 Datasets~~~~

The ~~Temperature~~ T and ~~water vapor mass mixing ratio~~ q profiles are derived from high-spectral-resolution observations made by the Atmospheric Infrared Sounder (AIRS) (Aumann et al., 2003; Chahine et al., 2006) onboard the Aqua spacecraft (Parkinson, 2003). The Aqua ~~spacecraft~~ satellite is ~~part~~ one of the Earth Observing System (EOS) satellites and shares its near-polar (98° inclination) orbit with the other satellites that form the afternoon ~~satellite constellation~~ A-Train constellation (Stephens

et al., 2008). ~~It~~ Aqua orbits the Earth at ~~a~~ ∼ 705 km altitude in a sun-synchronous ~~near-polar~~ orbit, ~~which means that it orbits from pole to pole~~ with an equatorial crossing ~~the equator at fixed times, i.e. around~~ of 1:30 p.m. (1:30 a.m.) local time ~~on~~ for ascending ~~(northwestwards) tracks and 1:30 a.m. on~~ (descending) ~~(southwestwards) tracks~~ orbital segments . With a swath width of 1650 km, the AIRS ~~which enables the~~ instruments ~~is~~ is able to provide a near-global daily coverage ~~each day~~.

2.1 Three types of AIRS-~~AMSU-HSB~~ standard retrievals

The AIRS instrument is a cross-track scanning spectrometer with ~~2,378 infrared (IR) channels that cover a spectral range from 3.7 to 15.4 μm. There are~~ 90 AIRS-IR ground footprints per swath ~~of~~ ∼ 1,650 km (depicted in Fig. 1 of Aumann et al. (2003)) and results in a horizontal resolution of 13.5 km at nadir view . ~~Additionally, the instrument has four visible and near infrared channels with ranges between 0.40 and 0.94 μm with a horizontal resolution of 2.28 km at nadir~~. The self-calibrating instrument enables the estimation of vertical profiles of several atmospheric variables (e.g., temperature, humidity) and minor gases (e.g., ozone, carbon dioxide) from the surface up to an altitude of 40 km with a quality approaching conventional radiosonde soundings and a vertical resolution of one kilometer (Chahine et al., 2006).

AIRS is accompanied by two synchronized and aligned microwave instruments . ~~:t~~ The Advanced Microwave Sounding Unit (AMSU) is a two-unit microwave radiometer with 15 channels that ~~are sensitive to~~ observe frequencies between 23 and 89 GHz~~, around the~~ including the 60 GHz oxygen band, ~~with~~ and a horizontal resolution of 45 km at nadir view. ~~and t~~The Humidity Sounder for Brazil (HSB) ~~,~~ is a four channel radiometer ~~sensitive to~~ that observes frequencies between 150 and 190 GHz, ~~concentrated~~ centering ~~around~~ on the 183 GHz water vapor line, ~~with~~ and has a horizontal resolution of 13.5 km at nadir (Lambrigtsen and Calheiros, 2003).

The microwave instruments are used together with ~~to detect clouds and appropriately correct the~~ IR spectra by applying a process called *cloud clearing* (Susskind et al., 2003). During the process, the horizontal resolution is ~~reduced~~ coarsened from 13.5 km to 45 km because all of the variability in the ~~to obtain cloud-cleared spectra, each~~ AMSU footprint ~~is combined with~~ that contains nine co-aligned AIRS footprints is assumed to arise from cloud variations. The cloud-cleared spectra are then used to ~~derive~~ retrieve ~~temperature~~ T and ~~humidity~~ q profiles for three different instrument combinations: ~~in the AIRS-AMSU and~~ AIRS-AMSU-HSB, AIRS-AMSU, and AIRS-IR (also ~~called~~termed AIRS-only) the last of which does not use microwave channels but is still obtained at~~is a control product that does not use microwave instruments, but has~~ the same ~~horizontal~~ spatial resolution as ~~the~~ AIRS-AMSU and AIRS-AMSU-HSB ~~data products~~ (Chahine et al., 2006).

The three-instrument AIRS suite enables the estimation of three-dimensional (3D) atmospheric ~~fields~~ profiles along the orbit of Aqua, since 30 Aug. 2002 ~~to~~ until present (except until 5 Febr~~u~~ari 2003 for HSB). Swath measurements are ~~collected~~ organized in files that contain ~~every~~ six minutes of data (Level 2) and are termed a 'granule~~s~~'. ~~Every~~ Each day ~~there are~~ 240 granules ~~available~~ are produced, each consisting of 30 times 45 ~~fields or~~ vertical profiles of T and q. ~~depending on the variable under consideration.~~ Fig. 1a displays an AIRS-AMSU-HSB Version 6 (v6) temperature field at 500 hPa in the very first granule that is available at NASA Goddard Earth Sciences (GES) Data and Information Services Center (DISC). Further Details about the AIRSv6 datasets ~~can be~~ are found in Susskind et al. (2014).

2.2 AIRS infrared-only Optimal Estimation (AIRS-OE)

Other alternative ~~M~~methods are ~~being developed~~ undergoing development ~~to deal with~~ that treat clouds during the retrieval process in a more sophisticated approach without reducing the horizontal resolution of the ~~temperature~~ T and ~~humidity~~ q fields that are ~~retrieved with an infrared sounder~~ described in Chahine et al. (2006) . The Optimal Estimation OE retrieval system for AIRS (AIRS-OE) ~~, introduced~~ is described by Irion et al. (2018) ~~, is such a method and its temperature~~ and ~~humidity derived fields are~~ is used ~~here~~ in addition to the three coarser-resolution AIRS data products described ~~in the~~ previously ~~subsection~~. ~~In their method, which~~ The methodology is based on ~~retrieval methods~~ the works of Bowman et al. (2006) and Rodgers (2000). Cloud detection and cloud property estimation ~~have been performed using~~ is enhanced with coincident high spatial resolution imaging data from the Moderate Resolution Imaging Spectroradiometer (MODIS) instrument ~~, a 36-channel cross-track scanning radiometer measuring visible and infrared radiation in a spectral range from 0.415 to 14.235 μm~~ with a horizontal resolution of ~~250-1,000 m~~ 0.25-1.0 km ~~at nadir~~ and a swath width of 2,330 km and also resides ~~onboard~~ on EOS Aqua ~~spacecraft~~ with AIRS (King et al., 2003; Parkinson, 2003; Platnick et al., 2003).

3 Methodology

~~Instead of calculating power spectra and measuring slopes within the diagrams, in~~ Our ~~method~~ approach is to calculate standard deviations as a function of length scale, then ~~are used to calculate~~ scaling exponents are calculated that correspond~~ing~~ to a particular range ~~of~~ in length scales (as in KT09). ~~In this paper, t~~The scaling exponents obtained using standard deviations are referred to as "variance scaling" exponents.

If a power-law relation exists between the standard deviation and the length scale, then given two length scales $l_1 < l_2$ with standard deviations σ_1 and σ_2, the scaling exponent α is:

$$\alpha = \frac{\ln(\sigma_2) - \ln(\sigma_1)}{\ln(l_2) - \ln(l_1)}.$$

When plotting the standard deviation as a function of length scale, while using logarithmically scaled horizontal and vertical axes, the scaling exponent α determines the slope of the line from (l_1, σ_1) and (l_2, σ_2). This line is straight if a power-law relation exists and is half as steep as for variances, which can equivalently be used instead of standard deviations to calculate the variance scaling exponents (Vogelzang et al., 2015).

~~Analogously to~~ Following KT09, ~~in this paper~~ α_L is defined as the "large-scale" scaling exponent for ~~length~~ scales between 6° and 12°, and α_S is defined as the "smal-scale" exponent for ~~length~~ scales between 1.5° and 4°. In addition, we added a third exponent α_T that is defined as the scaling exponent for "tiny" length scales between 0.5° and 1.5°. The length scales ~~are~~ is expressed in degrees over great circles. ~~and are assumed to not change with latitude or longitude~~. To ~~connect~~ relate the computed α values to the more commonly used power spectral ~~line slopes~~ exponents β, α values are ~~converted~~ interchanged with ~~in~~ β values by using the following equation (KT09, Davis et al. 1996 and Yu et al.(2017)):

$$\beta = -(2\alpha + 1). \tag{1}$$

The well-known $\beta = -5/3$ and $\beta = -3$ correspond to $\alpha = 1/3$ and $\alpha = 1$, respectively. ~~The next subsection~~ Below ~~gives~~ we describe ~~a description of~~ the estimation of standard deviations ~~along~~ within the AIRS swath following the ground track of Aqua.

3.1 Circular ~~approach~~ geometry

Standard deviations are computed ~~over~~ within circular areas ~~with~~ of diameter l. The ~~largest~~ maximum length scale is determined by the fixed swath width of AIRS, $L = 15.4°$. In that limiting case, a circle with radius $7.7°$ is positioned with its center ~~at~~ on Aqua's track (at nadir) after which the standard deviation of ~~the~~ valid ~~temperature~~ T and ~~water vapor~~ q values ~~that~~ are ~~inside it are~~ calculated within the circle . A depiction of ~~a water vapor field at~~ the 500 hPa q using AIRS-OE-retrievals that are inside a ~~circle with~~ $15.4°$ diameter circle is ~~presented~~ found in Fig. 2a. The smallest length scale is the other limiting case and is determined by the horizontal resolution of the observations. Here, we require that the minimum number of valid retrievals that are ~~required~~ necessary to ~~get~~ calculate a ~~(contributing)~~ standard deviation from a circle with a given diameter is five, as assumed in KT09. Taking this requirement into consideration, for AIRS-OE retrievals the smallest length scale, and hence the smallest diameter of the circles is chosen to be $l = 0.5°$. For the three coarser-resolution AIRSv6 data products (AIRS-IR, AIRS-AMSU, AIRS-AMSU-HSB) the smallest length scale is chosen to be $l = 1.5°$.

3.2 Monte Carlo ~~method~~ calculations

To obtain the standard deviations corresponding to length scales smaller than $L = 15.4°$ (i.e. $0.5° \leq l < 15.4°$), smaller circles are randomly placed inside the largest circle ~~with diameter 15.4°~~. So, the radius of the circle is reduced to obtain standard deviations corresponding to smaller length scales l. Given that a smaller circle with diameter $l < 15.4°$~~, it~~ is randomly placed ~~at a random location inside~~ within the largest circle, we further require that the smallest circle ~~and such that it~~ is entirely ~~inside it~~ within the larger circle. Then, ~~and~~ the standard deviation of ~~the temperature~~ T ~~or~~ and q ~~water vapor~~ values that are located ~~in~~ within the smaller circle are computed.

~~In order to get~~ To obtain a ~~better~~ more robust estimate, a *Monte-Carlo* estimation procedure is employed. The random placement is repeated 10,000 times for each of the smaller circle diameters. ~~which means that 10,000 circles are placed randomly inside the largest circle, and their~~ The average standard deviation over all 10,0000 values is used as ~~an~~ the estimate of the standard deviation corresponding to ~~the length scale~~ l. ~~A subtle note on random placement: this~~ The random placement should be done such that the 10,000 smaller circles cover the largest circle as uniformly as possible . This procedure is repeated for all length scales $0.5° \leq l < 15.4°$ for AIRS-OE ~~for (~~ and down to $1.5°$ ~~when using~~ for AIRSv6 products. Two out of these 10,000 smaller ~~($l = 6°$)~~ circles at $l = 6°$~~that are entirely contained in the 15.4°-diameter circle~~ are displayed in Fig. 2b.

3.3 Along-track instantaneous variance scaling ~~along the track~~estimates

~~A special feature of the~~ The intent of this method is ~~that~~ to move the $15.4°$ diameter circle ~~can move~~ along with the orbit of the Aqua satellite ~~. To be precise, its center can move along with the track of the orbits nadir~~ to estimate standard deviations and

~~hence~~ therefore ~~the~~ variance scaling exponents at each successive scan line along the satellite ground ~~of a horizontal circular area around the~~ track. This ~~works fine as long as circles are entirely contained in a single granule. If the 15.4°-diameter circle is close to the edge and partly covers two granules, the two~~ requires stitching together successive granules. ~~can be glued together. By repeating this procedure of glueing granules,~~ Therefore, a novelty of this approach is that the variance scaling can be derived instantaneously ~~(i.e. without time averaging) along the track of the Aqua satellite and for as many granules as desired.~~ (i.e. no time averaging as in KT09) .

~~By varying the diameter of the circular areas, while covering the selected area in a uniform way, standard deviations can be estimated in the area under consideration.~~ The diameter of the circles can vary with arbitrary ~~small~~ increments; ~~and is chosen to vary with increments of~~ we select $0.5°$, which ~~gives a~~ should yield sufficient resolution to resolve scale-dependent breaks and other behavior introduced in Section 4. ~~in the variance-scaling plots that are introduced in Section 4~~. After the calculations of the standard deviations as a function of length scale, the three exponents (i.e. the slopes) are estimated by a least squares fit (Weisstein, 2017).

For α_L, the formula of Weisstein(2017) is:

$$\alpha_L = \frac{n\sum_{i=1}^{n}(\ln x_i \ln y_i) - \sum_{i=1}^{n}(\ln x_i)\sum_{i=1}^{n}(\ln y_i)}{n\sum_{i=1}^{n}(\ln x_i)^2 - (\sum_{i=1}^{n}\ln x_i)^2}, \tag{2}$$

where $x_i = l_i$ and $y_i = \sigma_i$, with $6° \leq l_i \leq 12°$ and $n = 13$. For α_S and α_T, the formula is used with $1.5° \leq l_i \leq 4°$ and $0.5° \leq l_i \leq 1.5°$ and $n = 6$ and $n = 3$.

~~Furthermore,~~ We note that β_L, β_S and β_T are the analogs of α_L, α_S and α_T and will ~~sometimes~~ be interchangeably used ~~instead of the~~ with α values~~, because the~~ as β values ~~, such as $\beta = -3$ and $\beta = -5/3$,~~ are more commonly used in the literature.

3.4 Scale break detection

To ~~examine~~ quantify the length scale l_b at which the ~~variance scaling~~ exponents change, ~~for example~~ (e.g., from ~~a~~ $\beta = -3$ to a $\beta = -5/3$) ~~slope,~~ the standard deviation as a function of ~~length scale~~ l is approximated by two power laws, which is equivalent to fitting two straight lines optimally in a double-log scaled figure. When using the higher spatial resolution AIRS-OE ~~data product~~ retrieval, ~~which covers a larger range of scales,~~ the double scale break is examined by fitting three straight lines in the variance scaling plots. To do this optimally, we iterate over all possible (double) scale break positions $l \in \{1°, 1.5°, \ldots, 15°\}$ ~~are calculated~~ to find the two (three) ~~straight~~ fitted lines that minimize the ~~error with the data~~ the sum of the squares of the vertical offsets from the data to the lines. Since such a minimum always exists, albeit very subtle at times, we find an optimal single scale break l in each variance scaling diagram for AIRS-AMSU-HSB, AIRS-AMSU, and AIRS-IR, and two scale break values of l for AIRS-OE. In future work, thresholds could be used to make a distinction between variance scaling diagrams with and without scale breaks. .

4 Results

4.1 Variance scaling diagrams

To demonstrate the methodology, we ~~The~~ aim ~~is~~ to construct variance scaling diagrams that are ~~similar~~ analogous to Fig. 3 of Nastrom and Gage (1985). In this work, Fig. 3 ~~displays~~ shows the standard deviations of ~~the temperatures at~~ 500 hPa T at four selected locations on the ~~track of~~ Aqua track . ~~calculated with circular areas within four 15.4°-diameter circles having their centers on the track.~~ The four locations are chosen because ~~their diagrams give an overview of~~ they encompass typical behavior of the scaling. ~~but~~ We note that the ~~precise~~ scaling ~~patterns~~ behavior ~~can change~~ drastically changes at these locations depending on the ~~atmospheric circumstances~~ day . The four available AIRS retrievals ~~data products~~ are ~~included~~ shown in order to ~~get~~ gain insight regarding the uncertainty of the scaling that arises from sampling, retrieval algorithm, and observation frequency ~~an impression of the uncertainty of these scaling diagrams due to sampling~~ differences.

The standard deviation ~~usually~~ typically increases as a function of ~~length scale~~ l, only in Fig. 3c do we find that the standard deviation decreases at ~~the~~ larger ~~length scales~~ l for ~~when~~ AIRS-OE ~~is used~~. In Fig. 3a, this increase is not constant: at ~~the~~ larger ~~scales~~ l, ~~it is close to~~ $\beta = -3$ while ~~and~~ at ~~the~~ smaller ~~scales~~ l, ~~β increases up to~~ $\beta = -5/3$ for AIRS-OE. In ~~this panel~~ Fig. 3a, the slope changes between ~~the length scales~~ $l = 9°$ and $l = 11°$, ~~which~~ and is ~~an~~ clear example of a well-behaved scale break. Observe ~~that~~ in Fig. 3c that the slope at ~~the~~ smaller ~~scales~~ l is steeper than at the larger ~~scales~~ l, and ~~which~~ is an example of a reverse scale break ~~which has been~~previously reported ~~before by~~ in KT09 for specific humidity. In Fig. 3d, there is no clear scale break at all except for some small wiggles in the spectra.

The differences ~~of~~ in the standard deviations ~~between~~ among the three coarser-resolution AIRS data products are generally small and ~~differences that arise can partly be~~ are partly attributed to ~~blocking~~ sampling differences from clouds. AIRS-OE ~~tends to give~~ generally yields higher standard deviations, most notably in Fig. 3b, which is to be expected because of ~~its~~ the higher spatial resolution. ~~Further~~ Other contributions to discrepancies among the retrievals ~~can partly~~ may be attributed to spatial sampling differences that arise from differences in the spatial distributions of unsuccessful retrievals. Given that the variance of T and q is highly location dependent, the additional sampling provided by the microwave frequencies also will lead to differences in the four retrievals in Fig. 3. ~~gaps in the temperature or water vapor fields due to unsuccessful retrievals (e.g. of low quality) mostly in AIRS-OE.~~ Observe that the relative differences between the slopes of the four ~~lines~~ different retrievals appear to be , ~~which are of main interest, are~~ smaller than the ~~relative~~ magnitude differences ~~in the actual values~~ themselves .

The corresponding ~~moisture plots~~ q spectra at 500 hPa are ~~given~~ shown in Fig. 4. The scaling ~~diagram~~ of q in Fig. 4a is similar to ~~the temperature diagram~~ scaling in T in Fig. 3a ; however, ~~but~~ the slopes ~~are even~~ appear to be closer to $\beta = -5/3$ at the smaller l in Fig. 4a. In Fig. 4b, ~~the~~ a reverse scale break is clearly visible ~~around~~ near $l = 9°$. In Fig. 4c, the discrepancies between the four ~~data products~~ retrievals are more significant at ~~the~~ larger ~~scales~~ l , where AIRS-OE ~~displays~~ shows a decreasing standard deviation as a function of ~~length scale~~ increasing l. However, the AIRS-OE with a peak around 8° may be a result of finer-scale fluctuations that are only captured by AIRS-OE. At ~~the~~ smaller scales, the slopes are similar and reside between $\beta = -3$ and $\beta = -5/3$. In Fig. 4d, ~~all~~ the slopes are close to $\beta = -3$ at ~~the~~ larger l ~~scales~~, then ~~slowly increase~~ are close to $\beta = -1$ (i.e. $\alpha = 0$) around $l = 7°$, then again increase and decrease ~~again~~ at smaller length scales, in sharp contrast to T in Fig. 3d.

4.2 Along-track Variance scaling ~~along the track~~

~~Instead of plotting the entire variance scaling diagram as has been done in the previous subsection, here the~~ We now focus on the scaling exponents α_L, α_S and α_T, along 84 min of the Aqua track ~~The center of the 15.4°-diameter circle is positioned at Aqua's nadir at the first swath of~~ starting at the second granule ~~that is~~ available in the ~~database~~ AIRS archive. We ~~estimating~~ estimate scaling exponents ~~of the temperature and water vapor at~~ 500 hPa T and q. ~~Note that this~~ The 84 min dataset is a very small subset of the ~~entire multi-year (~~$\sim$ 15 year~~)~~ AIRS dataset and corresponds to just under one complete orbit. The centers of consecutive 15.4° diameter circles are ~~chosen to be~~ 8 seconds apart from each other, corresponding to the time it takes to make ~~one~~ 30 AIRS-AMSU soundings along the width of the swath. ~~swath (i.e. 6 min divided by 45 swaths).~~ As consecutive 15.4° circular areas have high ~~Due to~~ overlap, there are ~~strong~~ large correlations ~~between the~~ in exponents ~~calculated on consecutive circular areas along the track.~~ along neighboring scan lines.

~~Fig. 5a displays~~ The three scaling exponents derived from AIRS-OE ~~temperature~~ retrievals are shown in Fig. 5a. Observe that the exponent α_L fluctuates between ~~$\alpha =$~~ 0 and ~~$\alpha =$~~ 1 (left ~~reversed~~ vertical axis) ~~which~~ that corresponds to β values between ~~$\beta =$~~ -1 and ~~$\beta =$~~ -3 (right vertical axis). The exponent α_S has smaller fluctuations ~~fluctuates~~ around $\alpha = 1/3$ ~~corresponding to~~ ($\beta = -5/3$). The exponent α_T exhibits even ~~has a slightly~~ smaller fluctuations ~~range~~ than α_S and ~~stays~~ usually resides between ~~$\alpha =$~~ 1/2 and ~~$\alpha =$~~ 1/3, and correspond~~sing~~ to β between -2 and $-5/3$.

The standard deviation estimates from which these scaling exponents are calculated are shown in Fig. 5b. The lowest line is the standard deviation corresponding to $l = 0.5°$, the line above ~~it is the standard deviation~~ correspond~~sing~~ to $l = 1.0°$, and so forth. ~~It is clear that~~ The standard deviations are usually, but not always,increasing as a function of length scale.

~~Notable is that the~~ Local maxima~~um values~~ of the standard deviation ~~of~~ at 15.4° ~~tend to~~ co-align with ~~the~~ local maxima~~um values~~ of α_L (~~corresponding to the~~ local minima~~um values near~~ of $\beta = -3$). A large standard deviation at ~~the larger~~ synoptic scales is indicatesive of meridional ~~that there is a large-scale slope in~~ temperature gradients along the satellite track, which correlates ~~strongly~~ well with α_L ~~as will be~~ (shown later). ~~The location on Earth can be derived from~~ The latitude and longitude at nadir are depicted in Fig. 5c. ~~which displays the longitude and latitude of Aqua's nadir, which is the center of the 15.4°-diameter circle.~~

~~A large~~ Increased separation ~~of~~ between the three values of α in Fig. 5a, ~~indicates a large difference in slopes and hence~~ suggest the existence of scale breaks at those latitudes. For example at time 75 min 40°S, ~~the large-scale exponent is close to~~ $\alpha = 1$ ($\beta = -3$), while $\alpha_S = 0.6$ and $\alpha_T = 0.5$. ~~are smaller, such that β increases at smaller length scales.~~ ~~Close~~ Nearer to the equator around 33 min, the ~~roles~~ estimates are reversed: ~~the large-scale exponent is close to zero~~ $\alpha_L = 0$, ~~the tiny scale exponent close to~~ $\alpha_T = 1/2$ and nearly unchanged, and α_S is ~~in the small-scale exponent~~ in between ~~these~~ the two other values of α, indicating ~~the existence of~~ a double reverse scale break (steeper exponents at smaller scales). ~~Just before 60 min~~ Around 58 min near Antartica, the three values of α are ~~almost~~ nearly equal ~~such that that there are~~ with no ~~clear~~ apparent scale breaks. ~~Its variance-scaling plot~~ Analogous variance scaling diagrams ~~will~~ would be similar to that shown in Fig. 3~~d for which the three values are almost equal as well (around 46 min)~~.

The corresponding ~~moisture~~ q~~scaling~~ exponents are shown in Fig. 6a. The ~~moisture~~ α_L ~~is in the same~~ has a similar range as the ~~temperature~~ T ~~large-scale~~ exponent. The ~~moisture small-scale exponent~~ α_S for q ~~has slightly~~ is slightly larger ~~values~~ than for ~~the temperature~~ T ~~equivalent~~. However, ~~T~~the ~~tiny-scale exponent~~ α_T for q is significantly ~~higher~~ larger ~~for moisture~~ than for ~~temperature~~ T . Fig. 6b ~~shows~~ depicts the standard deviations of ~~the water vapor mass mixing ratio~~ q . ~~It is clearly visible that I~~in the tropics (~~the~~ location ~~on Earth can again be derived~~ from Fig. 5c), the standard deviation ~~of the water vapor~~ is much larger than ~~outside~~ in the extratropics (e.g., compare ~~e.g.~~ granules 231 and ~~with granule~~ 235. ~~Local~~ M~~m~~aximum values of standard deviation are ~~again to some extent~~ generally co-aligned with ~~the local~~ maximum values of α_L.

4.3 Variance scaling at ~~several pressure levels~~ 850, 500, and 300 hPa

~~KT09 showed~~ Previous studies have demonstrated that the magnitude of scaling exponents ~~are (among other factors) sensitive to~~ depends on ~~the~~ the altitude ~~in the atmosphere~~, ~~the~~ surface type, and ~~the presence of~~ cloud~~s~~ cover . Therefore, we show variance scaling exponents ~~are calculated~~ along the same ~~track~~ orbit segment at three pressure levels (300 ~~hPa~~, 500 ~~hPa~~ and 850 hPa) ~~and displayed~~ in Fig. 7 for ~~temperature~~ T and in Fig. 8 for ~~moisture~~ q. The results are typically noisier at ~~the~~ lower pressure levels (e.g., compare Fig. 7c to Fig. 7a,b) ~~because there, the number of successful retrievals,~~ and is consistent with a reduction in the yield ~~, is lower~~ (percentage of successful retrievals).

The three coarser-resolution AIRS products ~~give comparable results~~ are similar when the yield is high. ~~t~~Therefore ~~of these three products~~ we show only AIRS-AMSU derived exponents ~~are shown~~ in Fig. 7 and Fig. 8. ~~In Fig. 7, it can be seen that t~~The ~~large-scale exponent~~ α_L (blue dash-dotted line) for ~~temperature~~ T fluctuates ~~roughly~~ between ~~$\alpha =$~~ 0 and ~~$\alpha =$~~ 1, ~~apart from a part at the lower~~ except for a portion of the 850 hPa pressure level (Fig. 7c) around the South Pole (granule 235) where the yield ~~happens to be~~ is exceptionally low. The small-scale exponent α_S (red solid line) fluctuates within a smaller range ~~from $\alpha = 0.25$ up to $\alpha = 0.75$ apart from the interval~~ except for a portion of 850 hPa around 24 min in which ~~it almost reaches~~ $\alpha_S = 1$ ~~at the lowest level 850 hPa~~.

~~The~~ A reverse scale break ~~around~~ in the tropics (granule 231) is clearly visible at 500 hPa and to a lesser extent at ~~the other levels~~ 850 and 300 hPa, which is ~~in agreement~~ consistent with ~~the results of~~ KT09. The scaling exponent α_T (cyan dashed line) ~~that is~~ derived from ~~the~~ AIRS-OE ~~product~~ fluctuates between $\alpha = 0.2$ ~~and~~ to $\alpha = 0.6$ ~~most of the~~ for all time segments at ~~all~~ the three pressure levels. ~~Sensitivities to the~~ Variations with surface type and cloud fraction (not shown ~~in the figures~~) are less obvious in Figs. 7 and 8 and become clearer only after averaging over long time series~~, which has been performed by~~ (e.g., KT09).

~~Observe that in Fig. 8 t~~The ~~moisture scaling exponents~~ values of α for q ~~fluctuate faster~~ exhibit more rapid along-track fluctuations ~~than the temperature scaling exponents~~ compared to T at ~~all~~ the three pressure levels. The ~~large-scale exponents~~ α_L for q fluctuates ~~again~~ between ~~$\alpha =$~~ 0 and ~~$\alpha =$~~ 1 in Fig. 8 . The ~~small-scale exponent~~ α_S for q is ~~in the same range as was the case for temperature~~ similar to T, but ~~the tiny-scale exponent~~ α_T for q is ~~more often~~ typically larger than ~~$\alpha =$~~ 0.5 (~~below~~ $\beta_{\equiv} < -2$) and has a larger dynamic range for ~~moisture~~ q than for ~~temperature~~ T (compare Fig. 7 and Fig. 8). In granule 233 at 300 hPa, α_T ~~even becomes much larger than~~ exceeds ~~$\alpha =$~~ 1 ~~, which means that the slope in the variance-scaling figure is steeper than~~ ($\beta_{\equiv} < -3$).

4.4 ~~Variance-scaling~~ Distributions of variance scaling exponents ~~statistics~~

~~Statistics~~ Histograms of ~~the scaling exponents of the temperature and water vapor at~~ α_L and α_S for 500 hPa T and q obtained from five days of Aqua orbits are shown in Fig. 9. ~~The probability density functions (PDFs) of the exponents are derived from five days of observations.~~ To increase the computational speed, ~~of the calculations~~ only 100 circles are used in the Monte Carlo ~~estimation~~ method described earlier, which ~~leading~~ leads to a ~~slightly~~ slight increase in the number of ~~too large~~ extreme values of ~~the exponents~~ α_L and α_S . ~~It can be seen that the large-scale exponents~~ The histograms of $\alpha_L$have ~~a~~ larger rangesthan ~~the small-scale exponents~~ α_S, both for ~~temperature~~ T and ~~water vapor~~ q . ~~Furthermore, the small-scale exponents~~ The α_S~~have~~ exhibit a more symmetric distributions and the ~~PDFs attain their~~ maximum number of values is ~~close to~~ near $\alpha = 0.5$.

The asymmetry of ~~the large-scale exponent distribution~~ α_L for ~~temperature~~ T is caused by ~~the~~ different values ~~of the exponent~~ in the extratropics and ~~outside the~~ tropics. In the tropics ~~this exponent~~ α_L ~~tends to be~~ is closer to 0, ~~and outside~~ while in the extratropics it is ~~often~~ closer to 1. The ~~small-scale exponent~~ values of α_S ~~does~~ not have ~~such~~ a strong latitude dependency and ~~therefore~~ thus ~~does not display such a skewed~~ the distribution is more symmetric. The ~~large-scale exponent~~ α_L for ~~water vapor~~ q is skewed in the ~~other~~ opposite direction compared to ~~than the temperature large-scale exponent~~ α_L for T , because α_L ~~tends to be~~ is closer to 1 in the tropics and ~~outside often~~ closer to 0 in the extratropics.

These ~~kind~~ types of statisticsal distributions are ~~very~~ valuable ~~to improve~~ for the development and evaluation of cloud parameterizations ~~that make use of~~ based on PDF schemes.This is ~~E~~ especially true ~~the distribution of~~ for α_T (not shown); ~~,~~ ~~which is not shown, because~~ the AIRS-OE ~~data product~~ retrieval methodology is ~~still~~ in ~~preparation~~ developments and the ~~16 granules form too small a dataset to make reliable statistics~~ sample size from the limited set of granules is unable to yield a robust histogram. ~~The statistics that are shown, are intended to be an example of what is possible with~~ Our intent is to instead demonstrate the new scaling approach ~~combined with AIRS datasets~~. ~~Producing reliable statistics with the AIRS dataset, for example derived from 15 years of observations and using the method with 10,000 circles instead of 100, lies out of the scope of this paper that mainly introduces the new circular variance scaling approach.~~ A much larger and statistically robust dataset is outside the scope of this work. Furthermore, the computational expense is excessive using the Monte Carlo methodology with 10,000 circles rather than 100, and new ways of improving the speed of the calculations remains necessary.

4.5 Correlation ~~analysis~~ of scaling exponents to other quantities

To relate ~~the variance-scaling exponents~~ β_L and β_S to geophysical quantities,~~a~~ correlation analysis is performed using AIRS-AMSU retrieval and the results are ~~shown~~ summarized in Fig. 10. ~~The~~ A total number of 686 values (~~corresponding to~~ the ~~same~~ number of L2 retrieval swaths) cover a slightly ~~larger part of the track~~ longer extent of the orbital segment than the 84 min ~~segment~~ portion ~~that was~~ used in subsections 4.2 and 4.3. The ~~strongest~~ largest correlation coefficient (r) is found between ~~the large-scale exponent~~ β_L and the ~~absolute value of the mean temperature change (the slope)~~ mean T gradient in the along-track direction ~~of the track~~ of Aqua at nadir view (Fig. 10a). The ~~temperature~~ T change ~~that is~~ we considered is the difference between the average ~~temperature at~~ 500 hPa T ~~measured~~ over consecutive $15.4°$ diameter circles ~~(which centers are 8 seconds~~

~~apart from each other~~). If ~~there is a large temperature slope~~ the T gradient is large,~~then the exponent tends to be~~ β_L is closer to -3. If ~~there is no slope~~ the T gradient is small or near zero, ~~the exponent~~ β_L is closer to -1.

The ~~large-scale exponent~~ β_L ~~is~~ also ~~well-~~correlate~~s~~~~ed~~ strongly with the standard deviation of T in the $15.4°$ diameter circle (Fig. 10b), ~~which~~ this confirms the co-alignment of peaks observed in Fig. 5a and b. For ~~moisture~~ q, β_L is moderately ~~correlations are found between α_L and~~ correlated with the standard deviation in the $15.4°$ diameter circle (Fig. 10d) and the ~~absolute value of the moisture slope along the track~~ along-track q gradient (Fig. 10e). The exponents β_L and β_S are positively correlated for both ~~temperature~~ T (Fig. 10c) and ~~water vapor~~ q (Fig. 10f) , but the correlations are notably larger for T . The surface type (land ~~or~~ versus ocean) is not strongly correlated with ~~the temperature or moisture large-scale scaling exponents~~ β_L or β_S~~at the lower pressure level 850~~ hPa (not shown). ~~Finally~~ Lastly, the cloud fraction ~~does not show strong correlations~~ has a rather weak correlation with ~~the scaling exponents~~ β_L and β_S at 500 hPa; again, a larger sample size may yield different results.

4.6 Scale break detection results

Fig. 11 ~~presents~~ shows an example of the methodology to detect scale breaks ~~detection results~~. ~~From these two plots it is already~~ This example makes it clear that the length scale of scale breaks ~~length scale~~ varies ~~significantly~~ substantially along the Aqua tracks . The ~~length scale of the scale break~~ l_b ~~in the top panel is two times larger than in the bottom~~ differ by a factor of two ~~panel~~ ($9°$ and $4.5°$, respectively). ~~The scale-break length scale~~ l_b fluctuates ~~heavily between $2°$ and $15°$~~ by an order of magnitude between $1.5°$ and $15°$along the Aqua track ~~of Aqua~~ at ~~the three pressure levels~~ 850, 500 and 300 hPa for all AIRS ~~data~~ retrieval products, and both for ~~temperature~~ T and ~~water vapor~~ q ~~(not shown in figure)~~.

~~To get more insight in the distribution of the scale-break length scale, probability density functions (~~ We show PDFs ~~are shown~~ in Fig. 12 to gain additional insight in the distributions of l_b. ~~To produce these PDFs the range of AIRS-OE is set to $1.5° \leq l \leq 15.4°$ such that it has the same range as the three other AIRS data products.~~ The resolution of AIRS-OE is fixed to $1.5° \leq l \leq 15.4°$ such that similar scale breaks will be detected as the three standard AIRS data retrievals. . The maximum frequency of occurence in the PDFs is ~~attained~~ between $7°$ ~~(i.e. $\sim$ 770 km)~~ and $10.5°$ for ~~temperature~~ T and between $5°$ and $8°$ for ~~water vapor~~ q at 850 hPa (Fig. 12e,f), between $8°$ and $11°$ for ~~temperature~~ T at 500 hPa (Fig. 12c) and around $9°$ for ~~water vapor~~ q at 500 hPa (Fig. 12d), between $5.5°$ and $9°$ for ~~temperature~~ T at 300 hPa (Fig. 12a) and around $9°$ for ~~water vapor~~ q at 300 hPa (Fig. 12b)~~,~~. These results,~~which is~~ to some extent, are in agreement with 500-700 km and 450-750 km l_b ~~scale break length scales~~ reported by Gage and Nastrom (1985) and Tung and Orlando (2003), respectively. The PDFs of ~~temperature~~ T (Fig. 12a,c) have ~~a~~ less well-defined ~~maximum~~ maxima compared to ~~than water vapor~~ q (Fig. 12b,d,f), ~~apart from temperature~~ except for T at 850 hPa (Fig. 12e), in which a clear peak is ~~visible~~ apparent at ~~around~~ $7°$ (Fig. 12e) for three AIRS standard retrieval products.~~In the next section we provide a~~ A tentative physical and algorithmic explanation for the large spread of ~~the scale-break length scale.~~ l_b is provided in Section 5.

~~Finally~~ Lastly, An example of a double scale break detection is applied to the AIRS-OE dataset ~~for its full range, i.e.~~ $0.5° \leq l \leq 15.4°$ for T and q in Fig. 13. ~~Temperature and water vapor examples are shown in Fig. 13.~~ This example once again ~~shows~~ demonstrates the variety of variance scaling that is potentially observable ~~can be observed~~ in the atmosphere.

~~Observe that~~ The slope in the spectrum ~~gets~~ is steeper at the smaller scales ~~(below~~ less than $1.5°$~~)~~. This behavior is ~~can be~~ of importance for cloud parameterizations ~~that are~~ based on PDF schemes. Less variance ~~is present~~ exists at the smaller scales than ~~is expected~~ what one obtains from a simple extrapolation of ~~the~~ exponents at ~~the~~ larger scales to ~~the~~ smaller scales; this ~~has been recognized as well by KT09 and~~ was previously shown with in situ aircraft observations in Kahn et al. (2011) in a limited region of the subtropical southeasterns Pacific Ocean.

5 Discussion and conclusions

~~We show that individual granules of satellite Level 2 data can quantify the variability of the atmosphere.~~ The scale-dependent variability of temperature (T) and specific humidity (q) is derived from Level 2 satellite swath data. ~~In particular, t~~The variance scaling ~~exponents~~ of ~~temperature~~ T and ~~water vapor mass mixing ratio~~ q ~~have been derived using~~ uses data ~~stemming~~ from the Atmospheric Infrared Sounder (AIRS; Chahine et al. (2006)) instrument suite onboard the Aqua satellite. While ~~T~~these exponents are frequently close to the canonical $\beta = -5/3$ and $\beta = -3$ values, ~~however,~~ deviations from these values are ~~very common~~ more the rule than the exception. The large-scale exponents β_L ~~, corresponding~~ that correspond to the length scales between $6°$ and $12°$ fluctuate between -3 and -1, respectively.

The precise value of ~~the large-scale exponent~~ β_L depends strongly on the standard deviation of ~~temperature~~ T and ~~water vapor~~ q ~~content on larger areas~~ within larger spatial areas. The synoptic-scale ~~temperature~~ T and ~~moisture~~ q ~~slope~~ gradient ~~along the track~~ in the along-track direction also ~~affects~~ impacts the magnitude of β_L . ~~the large-scale exponent.~~ When the large-scale fluctuations or gradient are ~~strong~~ large, then ~~the large-scale exponent is close to~~ $\beta \approx -3$~~., which is the preferred value in case there is a large slope in the temperature (water vapor) field along the track.~~ When ~~the~~ large scale ~~temperature~~ T fluctuations are ~~small~~ reduced such as in the tropics, and the atmosphere is dominated by small scale fluctuations, $\beta_L = -1$.~~,~~ ~~then smaller-scale fluctuations easily decrease this value to -1. This happens often~~ iIn the tropics,~~(e.g. Fig.7b, granule 231),~~ ~~where~~ small-scale Tfluctuations dominate because of the preponderance of ~~that are likely the result of~~ deep convection.~~, can be stronger than the large-scale fluctuations.~~ In contrast, large-scale q fluctuations are more dominant in proximity to and within the tropics, which results in $\beta_L \approx -3$. ~~for moisture, such large-scale slopes can be expected close to and in the tropics, because there moisture differences are large: we have indeed seen in Fig. 6 that $\beta = -3$ is not so common off the tropics for the large-scale water vapor exponent β_L.~~

The small-scale variance scaling exponents β_S~~,~~ that correspond~~ing~~ to length scales ~~from~~ between $1.5°$ to $4°$ are more often close to $\beta = -2$, and less often close to $\beta = -3$. By using recently developed retrievals from single-footprint AIRS data (Irion et al., 2018), we show that at the smaller scales from $0.5°$ to $1.5°$, the exponents β_T are closer to -2 for ~~temperature~~ T and ~~slightly lower (between~~ closer to -2 ~~and -3)~~ for ~~moisture~~ q. The PDFs of ~~the~~ small-scale ~~exponents~~ α_S ~~(Fig. 9) show~~ exhibit a maximum around ~~$\alpha = 0.5$~~ -2 for both ~~temperature~~ T and ~~water vapor~~ q . ~~which~~ this is ~~perhaps~~ somewhat ~~a surprise~~ surprising ~~if one expects these exponents to have a preferred value of close to $\alpha = 1/3$, i.e. $\beta = -5/3$~~ , since previous studies have suggested values closer to $-5/3$. ~~Variance scaling exponents that are close to $\beta = -2$, i.e. $\alpha = 0.5$, indicate that the variance~~

~~of the temperature is proportional to the length scale l. The preferred slope of $\beta = -2$ can, however, not be clearly explained by the authors.~~

Deviations from typical values of β (-5/3 and -3) have been reported in the literature previously (e.g. KT09). Lovejoy et al. (2008) show that exponents derived from drop sondes over the northern Pacific Ocean reside in between -5/3 and -3 and have strong height dependence. It was shown that the vertical exponents are not equal to the horizontal exponents, and suggests 3D anisotropy. Lovejoy et al. (2009) and Pinel et al. (2012) showed that scale breaks detected by in situ aircraft observations may be the result of 3D anisotropy in atmospheric properties. In Pinel et al. (2012), scale breaks are observed in the 100 - 500 km range with horizontal exponents that transition from -5/3 to -2.4. In the vertical direction, an exponent of -2.4 is derived and suggests that gently sloping isobaric aircraft trajectories are the source of the transition to -2.4. Since the T and q exponents reside on isobaric surfaces (e.g. 500 hPa) in this work, one may expect that the vertical exponents may alias into the large-scale horizontal exponent. However, we do not find a clear indication of $\beta_L = -2.4$, although a focused effort on obtaining vertical scaling exponents with satellite soundings warrants further investigation. Unfortunately, the relative coarse vertical resolution of ~ 2 km from AIRS retrievals is not ideal for obtaining reliable estimates of vertical scaling exponents; dropsondes and radiosondes remain the standard and are much better suited to this observational challenge.

~~A special feature of the method is the usage of~~ The methodology described uses circles to calculate ~~the~~ standard deviations. ~~It is an interesting question what the shape of an area should be if one aims to estimate the variance scaling in the atmosphere at a certain pressure level.~~ The optimal shape of an area used to calculate variance remains an open question.Rectangles have been previously used ~~before,~~ (e.g. by KT09), and ~~have been~~ are generallyaccepted ~~by the community to be a correct shape to compute variance scaling exponents,~~ because ~~horizontal sections of~~ GCM columns ~~, for which variance-scaling exponents can be useful in cloud parameterizations,~~ are often (nearly) rectangular. The orientation of a rectangle or square should not be of major importance when calculating variance scaling exponents. ~~Therefore,~~ One could argue that ~~one could use a slight~~ incremental rotation of the rectangle about a central axis could be used to trace out the area of a circle. Within each rectangle, the variance can be calculated, and the same for each slight rotation of the rectangle about the center axis, until it is rotated 360°. ~~to calculate the variance scaling exponents and take the average of the values of the rotated and non-rotated rectangles. Then, the rectangle can be turned slightly again and again, while calculating scaling exponents. If one continues turning the rectangle, and makes the turning angles infinitesimally small, the resulting shape is a circle.~~ This procedure of incremental ~~rotating~~ rotation ~~can be~~ could be performed with any arbitrary shape. ~~with the circle as a~~ In all cases, the circle is the final result, and therefore one may conclude that the circle is the "optimal shape" to calculate variance scaling exponents. A circle is ~~It is~~ optimal in ~~case~~ the event that rotational symmetry is desired if , for example, ~~because~~ the underlying field is isotropic. This is ~~in line~~ consistent with Pressel and Collins (2012) who found that ~~water vapor~~ variance scaling of q is approximately isotropic.

A major advantage of ~~using~~ the ~~a~~ "poor man's spectral analysis" method (Lorenz, 1979) is that relatively small datasets are sufficient to estimate variance scaling exponents. Reliable spectral power diagrams of observational data arise only after averaging over relatively large datasets. For ~~example~~ instance, Nastrom and Gage (1985) obtained their spectral power diagrams by averaging over observations collected during 6,000 commercial aircraft flights. ~~Furthermore,~~ The calculation of spatial

variances ~~can be calculated~~ is still possible in the ~~case~~ event of missing or poor quality data, in which case conventional spectral analysis cannot be employed Vogelzang et al. (2015).

~~In this study,~~ The variance scaling exponents ~~have been~~ are computed nearly instantaneously without using multiple satellite overpasses (no time averaging) in this work. The exponents are derived from satellite observations ~~that are made during at most a few minutes~~ within a 15.4° diameter circle over a few minute time window, ~~so the scaling method is~~ thus ,strictly speaking,the method is "approximately" ~~not entirely~~ instantaneous. ~~However, compared to the months of measurements used by KT09 and Pressel et al. (2012) to compute exponents, our method uses relatively small datasets, which justifies the term instantaneous.~~ A result of ~~using these small datasets~~ the instantaneous approach is that ~~the~~ a much wider variety of scaling exponents is ~~large~~ revealed. The large variety of exponents is likely due to some extent from the turbulent structure of T and q fields with long-tailed non-Gaussian distributions (Tuck, 2010). These behaviors may inhibit the precise estimation of variance scaling exponents from observations. Further research is necessary to determine the impacts of the non-Gaussian distribution shapes of T and q on derived exponents, and their scale-dependence of non-Gaussianity. This effect likely contributes to spreading out the PDFs of exponents.

The ~~scale-break-detection~~ results ~~have~~ shown ~~that~~ there is a preference for ~~the~~ scale break length scales~~between~~ around 7° (at 850 hPa) and 9° (at 500 hPa and 300 hPa). This is slightly larger than the 500-700 km and 450-750 km ~~scale-brake length scales~~ reported by Gage and Nastrom (1985) and Tung and Orlando (2003), respectively, and smaller than ~~the~~ 1,000 km reported by Bacmeister et al. (1996). ~~Furthermore, as mentioned above,~~ Pinel et al. (2012) report ~~scale-break length scales~~ l_b between 100 km and 500 km. ~~In our results, t~~The spread around ~~this value~~ these values is large in our results and ~~this preference~~ a preferred length scale is only ~~visible in the distribution of the scale-break length scale, i.e. where the probability density function attains its maximum.~~ inferred from the maxima in the PDFs.An explanation for the large spread in the PDFs is that convective systems of different sizes exists ~~of all different sizes, thereby increasing the initially present slope of $\beta = -3$ to higher values at different length scales. A larger convective system will give a larger value of the scale-break length scale. In case no large-scale slope is present, the~~ The existence of a reverse scale-break ~~length scale~~ depends ~~also heavily on the size of the~~ on the scale of convective systems: the larger the ~~size~~ scale , the larger ~~the scale-break length scale~~ l_b . Furthermore, ~~since we measure scale-break length scales along the track~~ as l_b is obtained in the along-track dimension, for instance when the satellite observation transitions ~~moves~~ from a regime ~~where there is a scale-break at a small scale (say~~ with $l_b = 2°$) to a regime ~~where there is a scale-break at a large scale (say~~ with $l_b = 15°$), then ~~all~~ the intermediate ~~scale-break~~ length scales between 2° and 15° ~~will be attained during the overpass from the first to the second regime~~ are also retrieved in between the two regimes as the circular area advances along the swath.~~This explains the continuity of the scale-break length scale PDFs.~~ Due to the overlapping nature of the circular areas, this additionally smooths out the peaks in the PDFs, but further work is necessary to quantify the magnitude of this effect compared to the spreading due to non-Gaussianity.

The ~~variance-scaling~~ exponent β_T for ~~moisture~~ q ~~has been~~ was shown to attain smaller values, i.e. closer to $\beta = -3$ than the exponent β_S. ~~which~~ This means that less variance is present at ~~the~~ length scales between 0.5° and 1.5° than if extrapolated from exponents derived from ~~at~~ length scales between 1.5° and 4°. ~~, which has also been reported in Kahn et al. (2011). This can be of significance for parameterizations of clouds in GCMs that use assumptions about the variability of moisture content~~

~~at length scales below the grid scale, for example when a PDF method is used in the cloud parameterizations~~Scale breaks at subgrid scales in GCMs are of significance for cloud parameterizations in GCMs that extrapolate variability (Tompkins, 2002; Teixeira and Hogan, 2002; Teixeira and Reynolds, 2008).

~~Future work that is possible with the new variance scaling method presented here includes detailed examination of the variance scaling of cyclones at different stages of their life cycles, as has been performed with numerical simulations by Waite et al. (2013). This is possible because the method enables instantaneous derivation of the variance scaling diagrams. After locating the cyclones in satellite data and tracking them for a few days, the variance scaling diagrams can be computed for each stage of their development.~~ This novel instantaneous variance scaling methodology may enable detailed examination of the variance scaling of the time evolution of storm systems, such as extratropical cyclones at different stages in their lifecycle as previously demonstrated with numerical simulations by Waite and Snyder (2013), or with deep convection along the Mei-Yu front by Peng et al. (2014). The changes in the kinetic energy spectra in Waite and Snyder (2013) and Peng et al. (2014) occur on time scales of hours to several days. We postulate that scaling exponents derived from instantaneous snapshots obtained from satellite swath data will be useful observational constraints for time-dependent spectra generated from numerical modeling experiments. To conclude, it is well known that the time scale of predictability is closely linked to the spatial scale of the phenomenon of interest (Lorenz, 1969). In the case of moist baroclinic waves, steeper (shallower) spectral slopes at small scales for individual baroclinic waves are inherently more (less) predictable as the slope portrays the relative importance of convection within any given disturbance (Zhang et al., 2007). As a result, the instantaneous scaling exponents are expected to potentially offer a new type of observational constraint with relevance to the predictability of individual tropical or extratropical disturbances.

Data availability. The AIRS version 6 data sets were processed by and obtained from the Goddard Earth Services Data and Information Services Center (http://daac.gsfc.nasa.gov/). All rights reserved. Government sponsorship acknowledged.

Competing interests. The authors declare that they have no conflict of interest.

Acknowledgements. Part of this research was carried out at the Jet Propulsion Laboratory (JPL), California Institute of Technology, under a contract with the National Aeronautics and Space Administration. All authors were partially supported by the AIRS project at JPL.

References

Aumann, H. H., Chahine, M. T., Gautier, C., Goldberg, M. D., Kalnay, E., McMillin, L. M., Revercomb, H., Rosenkranz, P. W., Smith, W. L., Staelin, D. H., et al.: AIRS/AMSU/HSB on the Aqua mission: Design, science objectives, data products, and processing systems, IEEE T. Geosci. Remote, 41, 253–264, 2003.

Bacmeister, J. T., Eckermann, S. D., Newman, P. A., Lait, L., Chan, K. R., Loewenstein, M., Proffitt, M. H., and Gary, B. L.: Stratospheric horizontal wavenumber spectra of winds, potential temperature, and atmospheric tracers observed by high-altitude aircraft, J. Geophys. Res.-Atmos, 101, 9441–9470, 1996.

Bogenschutz, P. A. and Krueger, S. K.: A simplified pdf parameterization of subgrid-scale clouds and turbulence for cloud-resolving models, J. Adv. Model. Earth Sy., 5, 195–211, 2013.

Chahine, M. T., Pagano, T. S., Aumann, H. H., Atlas, R., Barnet, C., Blaisdell, J., Chen, L., Divakarla, M., Fetzer, E. J., Goldberg, M., et al.: AIRS: Improving Weather Forecasting and Providing New Data on Greenhouse Gases, Bull. Am. Meteorol. Soc, 87, 911–926, 2006.

Cusack, S., Edwards, J., and Kershaw, R.: Estimating the subgrid variance of saturation, and its parametrization for use in a GCM cloud scheme, Q. J. Royal Meteor. Soc., 125, 3057–3076, 1999.

Gage, K. and Nastrom, G.: On the spectrum of atmospheric velocity fluctuations seen by MST/ST radar and their interpretation, Radio Sci., 20, 1339–1347, 1985.

Hamilton, K., Takahashi, Y. O., and Ohfuchi, W.: Mesoscale spectrum of atmospheric motions investigated in a very fine resolution global general circulation model, J. Geophys. Res.-Atmos, 113, 2008.

Hunt, J. and Vassilicos, J.: Kolmogorov's contributions to the physical and geometrical understanding of small-scale turbulence and recent developments, Proc. R. Soc. Lond. A, 434, 183–210, 1991.

Irion, F. W., Kahn, B. H., Schreier, M. M., Fetzer, E. J., Fishbein, E., Fu, D., Kalmus, P., Wilson, R. C., Wong, S., and Yue, Q.: Single-footprint retrievals of temperature, water vapor and cloud properties from AIRS, Atmos. Meas. Tech., 11, 971, 2018.

Jonker, H. J., Duynkerke, P. G., and Cuijpers, J. W.: Mesoscale Fluctuations in Scalars Generated by Boundary Layer Convection, J. Atmos. Sci., 56, 801–808, 1999.

Julian, P. R., Washington, W. M., Hembree, L., and Ridley, C.: On the Spectral Distribution of Large-Scale Atmospheric Kinetic Energy, J. Atmos. Sci., 27, 376–387, 1970.

Kahn, B. H. and Teixeira, J.: A Global Climatology of Temperature and Water Vapor Variance Scaling from the Atmospheric Infrared Sounder, J. Clim, 22, 5558–5576, 2009.

Kahn, B. H., Teixeira, J., Fetzer, E., Gettelman, A., Hristova-Veleva, S., Huang, X., Kochanski, A., Köhler, M., Krueger, S., Wood, R., et al.: Temperature and Water Vapor Variance Scaling in Global Models: Comparisons to Satellite and Aircraft Data, J. Atmos. Sci., 68, 2156–2168, 2011.

King, M. D., Menzel, W. P., Kaufman, Y. J., Tanré, D., Gao, B.-C., Platnick, S., Ackerman, S. A., Remer, L. A., Pincus, R., and Hubanks, P. A.: Cloud and Aerosol Properties, Precipitable Water, and Profiles of Temperature and Water Vapor from MODIS, IEEE T. on Geosci. and Remote Sens., 41, 442–458, 2003.

Lambrigtsen, B. H. and Calheiros, R. V.: The Humidity Sounder for Brazil - An International Partnership, IEEE T. Geosci. Remote Sens., 41, 352–361, 2003.

Larson, V. E., Golaz, J.-C., and Cotton, W. R.: Small-Scale and Mesoscale Variability in Cloudy Boundary Layers: Joint Probability Density Functions, J. Atmos. Sci., 59, 3519–3539, 2002.

Lindborg, E.: Can the atmospheric kinetic energy spectrum be explained by two-dimensional turbulence?, J. Fluid Mech., 388, 259–288, 1999.

Lorenz, E. N.: Forced and Free Variations of Weather and Climate, J. Atmos. Sci., 36, 1367–1376, 1979.

Lovejoy, S. and Schertzer, D.: The weather and climate: emergent laws and multifractal cascades, Cambridge University Press, 2013.

Lovejoy, S., Tuck, A., Hovde, S., and Schertzer, D.: Do stable atmospheric layers exist?, Geophys. Res. Lett., 35, 2008.

Lovejoy, S., Tuck, A., Schertzer, D., and Hovde, S.: Reinterpreting aircraft measurements in anisotropic scaling turbulence, Atmospheric Chemistry and Physics, 9, 5007–5025, 2009.

Nastrom, G. and Gage, K. S.: A Climatology of Atmospheric Wavenumber Spectra of Wind and Temperature Observed by Commercial Aircraft, J. Atmos. Sci., 42, 950–960, 1985.

Palmer, T.: Towards the probabilistic Earth-system simulator: a vision for the future of climate and weather prediction, Q. J. Roy. Meteor. Soc., 138, 841–861, 2012.

Parkinson, C. L.: Aqua: An Earth-Observing Satellite Mission to Examine Water and Other Climate Variables, IEEE T. Geosci. Remote Sens., 41, 173–183, 2003.

Pinel, J., Lovejoy, S., Schertzer, D., and Tuck, A.: Joint horizontal-vertical anisotropic scaling, isobaric and isoheight wind statistics from aircraft data, Geophys Res. Lett., 39, 2012.

Platnick, S., King, M. D., Ackerman, S. A., Menzel, W. P., Baum, B. A., Riédi, J. C., and Frey, R. A.: The MODIS Cloud Products: Algorithms and Examples from Terra, IEEE T. Geosci. Remote Sens., 41, 459–473, 2003.

Pressel, K. G. and Collins, W. D.: First-Order Structure Function Analysis of Statistical Scale Invariance in the AIRS-Observed Water Vapor Field, J. Climate, 25, 5538–5555, 2012.

Stephens, G. L., Vane, D. G., Tanelli, S., Im, E., Durden, S., Rokey, M., Reinke, D., Partain, P., Mace, G. G., Austin, R., et al.: CloudSat mission: Performance and early science after the first year of operation, J. Geophys. Res.: Atmos., 113, 2008.

Susskind, J., Barnet, C. D., and Blaisdell, J. M.: Retrieval of Atmospheric and Surface Parameters From AIRS/AMSU/HSB Data in the Presence of Clouds, IEEE T. Geosci. Remote Sens., 41, 390–409, 2003.

Susskind, J., Blaisdell, J. M., and Iredell, L.: Improved methodology for surface and atmospheric soundings, error estimates, and quality control procedures: the atmospheric infrared sounder science team version-6 retrieval algorithm, J. Appli. Remote Sens., 8, 084 994, 2014.

Teixeira, J. and Hogan, T. F.: Boundary Layer Clouds in a Global Atmospheric Model: Simple Cloud Cover Parameterizations, J. Climate, 15, 1261–1276, 2002.

Teixeira, J. and Reynolds, C. A.: Stochastic Nature of Physical Parameterizations in Ensemble Prediction: A stochastic Convection Approach, Mon. Wea. Rev., 136, 483–496, 2008.

Tompkins, A. M.: A Prognostic Parameterization for the Subgrid-Scale Variability of Water Vapor and Clouds in Large-Scale Models and Its Use to Diagnose Cloud Cover, J. Atmos. Sci., 59, 1917–1942, 2002.

Tuck, A.: From molecules to meteorology via turbulent scale invariance, Q. J. Royal Meteorol. Soc, 136, 1125–1144, 2010.

Tung, K. K. and Orlando, W. W.: The k^{-3} and $k^{-5/3}$ Energy Spectrum of Atmospheric Turbulence: Quasigeostrophic Two-Level Model Simulation, J. Atmos. Sci., 60, 824–835, 2003.

Vogelzang, J., King, G. P., and Stoffelen, A.: Spatial variances of wind fields and their relation to second-order structure functions and spectra, J. Geophys. Res. Oceans, 120, 1048–1064, 2015.

Weisstein, E.: Least Squares Fitting-Power Law. From MathWorld–A Wolfram Web Resource, http://mathworld.wolfram.com/LeastSquaresFittingPowerLaw.html, 2017.

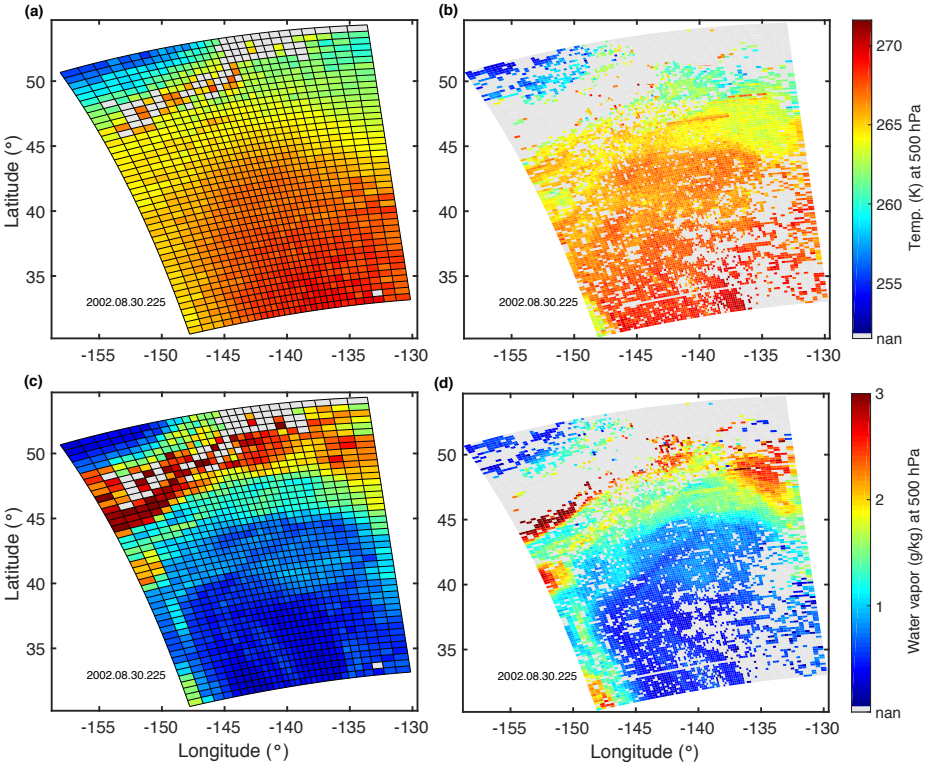

Figure 1. (a) Example of an AIRS-AMSU-HSBv6 temperature field at 500 hPa in a granule above the North Pacific Ocean - derived from soundings made during an ascending part of Aqua's orbit **(b)** the temperature field using AIRS-OE retrievals and **(c,d)** the corresponding moisture fields (the water vapor mass mixing ratio). Gray shading indicates that there was no acceptable retrieval.

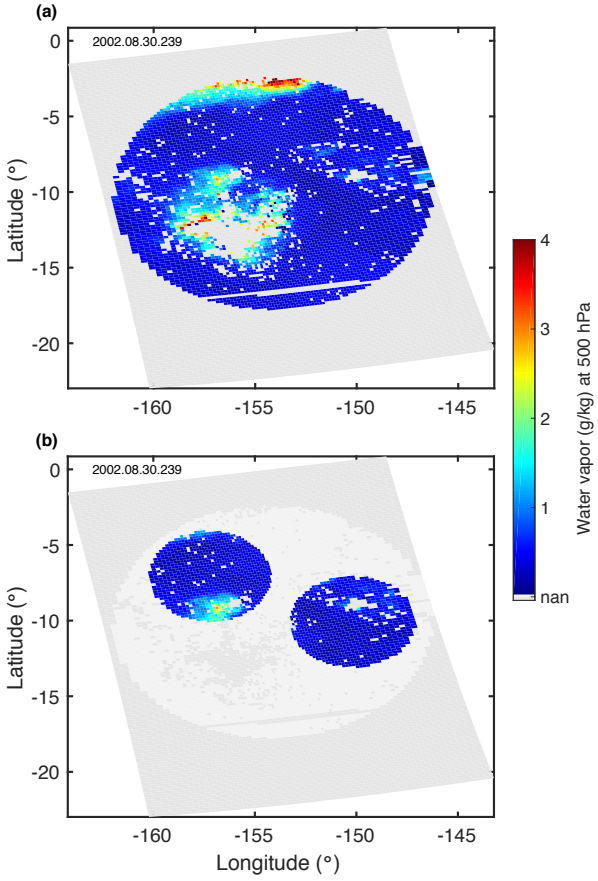

Figure 2. (a) Illustration of a water vapor mass mixing ratio field at 500 hPa using AIRS-OE retrievals that are inside a 15.4°-diameter circle and **(b)** inside two 6°-diameter circles. A dark gray shaded pixel inside a circle indicates that there was no acceptable water vapor content estimate. The granule, which is in an ascending part of Aqua's track above the South Pacific Ocean, has a relatively large yield (83%), however, it is clearly visible that atmospheric clouds are inhibiting retrievals around (156°W-13°S).

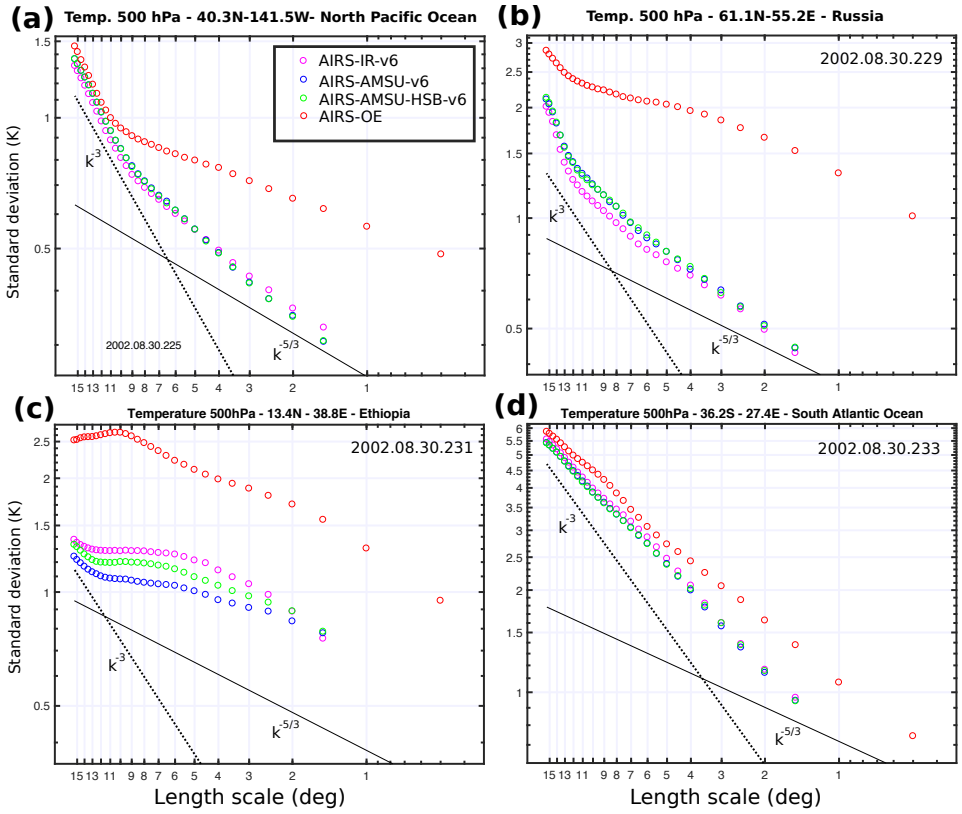

Figure 3. The standard deviation of the temperature at 500 hPa as a function of length scale l using AIRS-IR (magenta open circles), AIRS-AMSU (blue open circles), AIRS-AMSU-HSB (green open circles) and AIRS-OE (red open circles) on double logarithmic axes with the $\beta = -5/3$ slope (black solid line) and the $\beta = -3$ slope (black dotted line) in a circular area with a diameter of 15.4° located **(a)** in the North Pacific Ocean **(b)** in Russia **(c)** in Ethiopia and **(d)** in the South Atlantic Ocean.

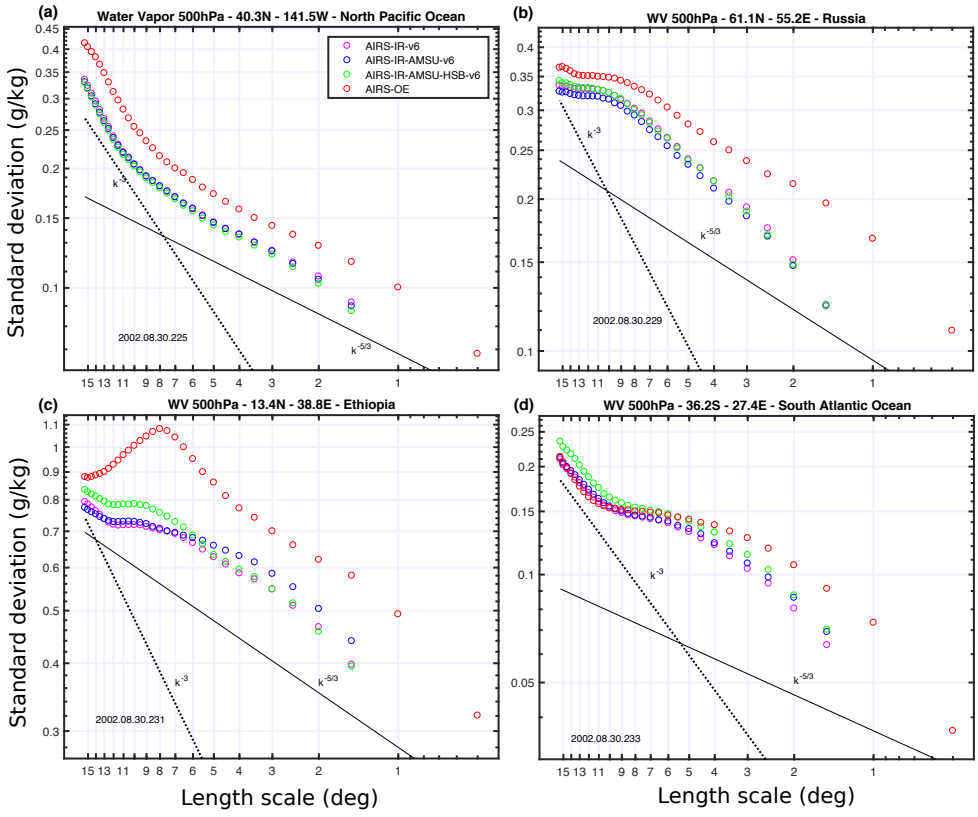

Figure 4. Same as Fig. 3 using the water vapor mass mixing ratio.

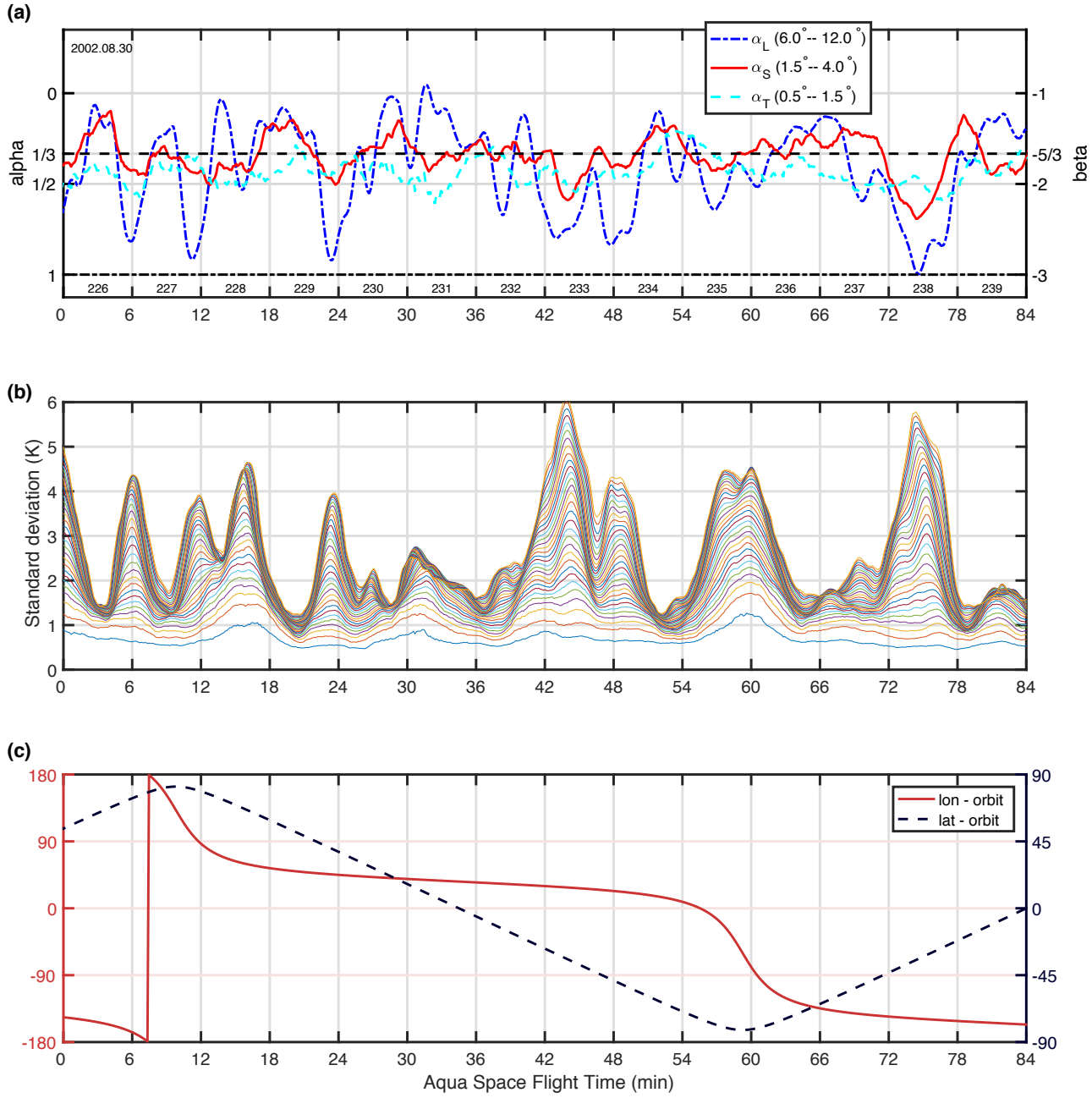

Figure 5. (a) AIRS-OE temperature 500 hPa variance scaling exponents α_L, α_S and α_T as a function of Aqua's flight time. The right axis displays the β value. **(b)** The standard deviations using length scales $l = 0.5°$ (lowest line) up to $L = 15.4°$ (usually the highest line) and **(c)** Aqua's longitude (left axis) and latitude (right axis).

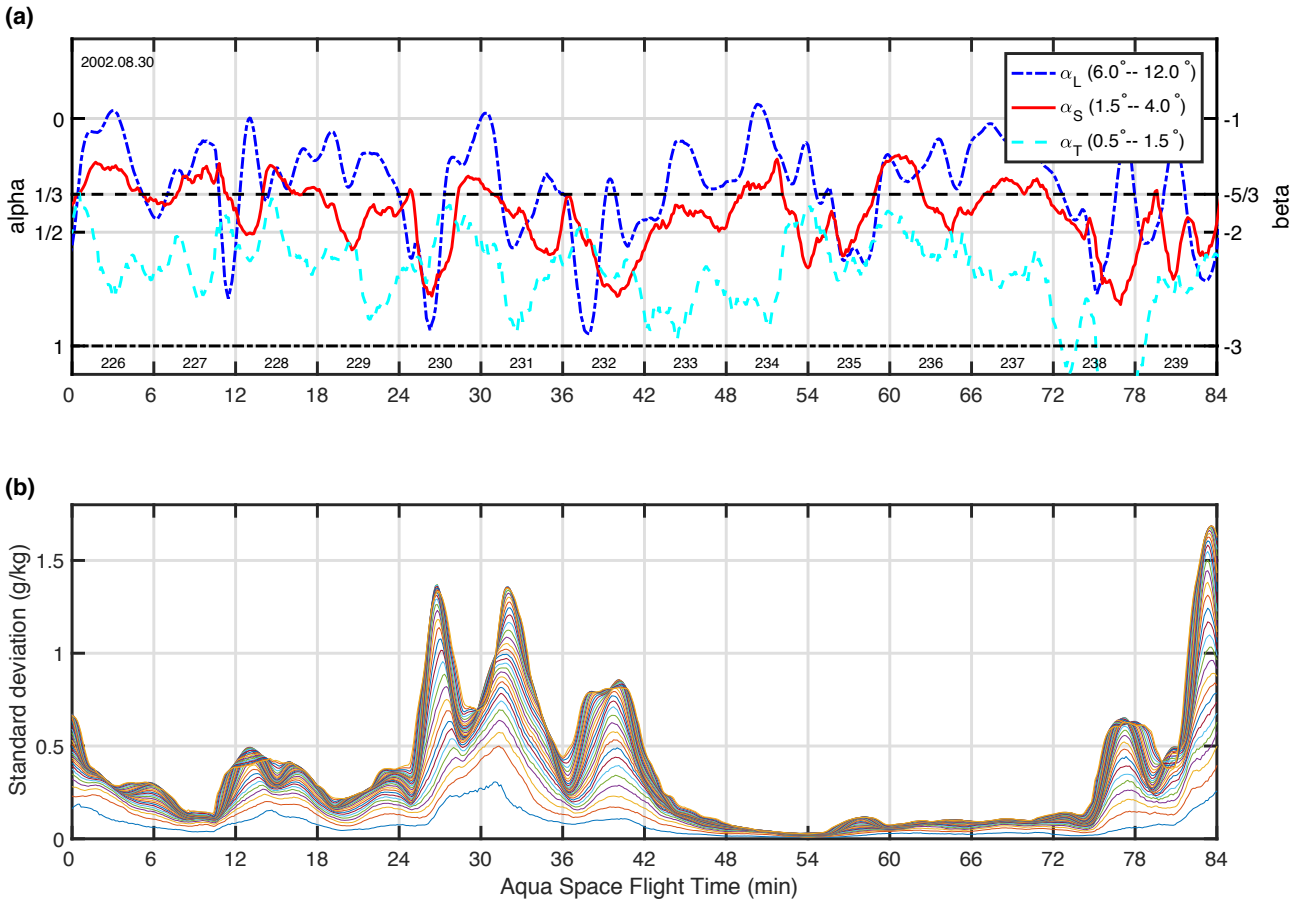

Figure 6. Same as Fig. 5 using the water vapor mass mixing ratio.

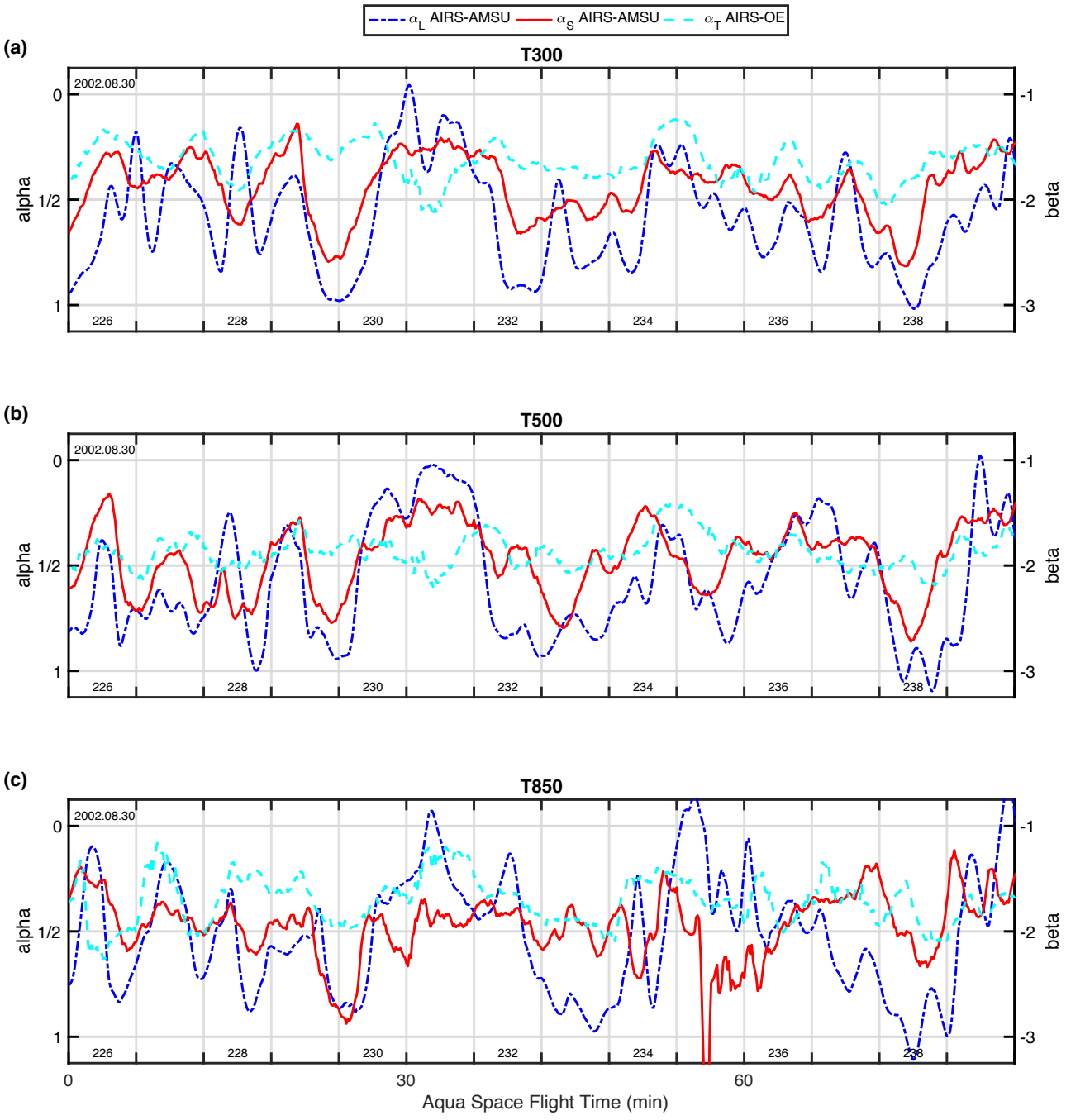

Figure 7. Variance scaling exponents α_L (blue lines), α_S (red lines) and α_T (cyan lines) as a function of Aqua's flight time for temperature **(a)** at 300 hPa **(b)** at 500 hPa and **(c)** at 850 hPa using AIRS-AMSU (α_L and α_S) and AIRS-OE (α_T). Additionally: the date (left upper corner) and granule numbers (bottom), the corresponding β values can be seen on the right axis.

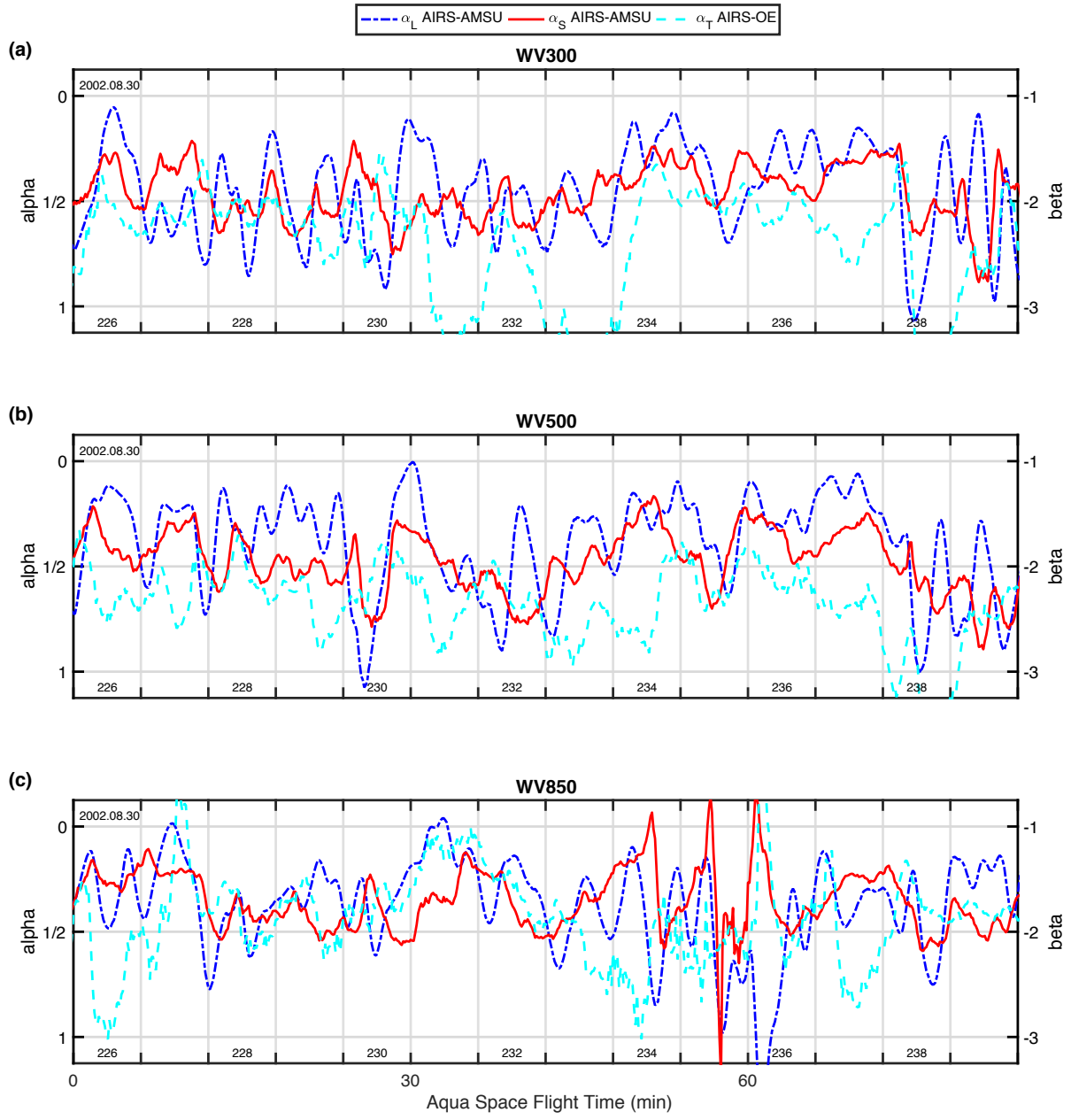

Figure 8. Same as Fig. 7 using the water vapor mass mixing ratio.

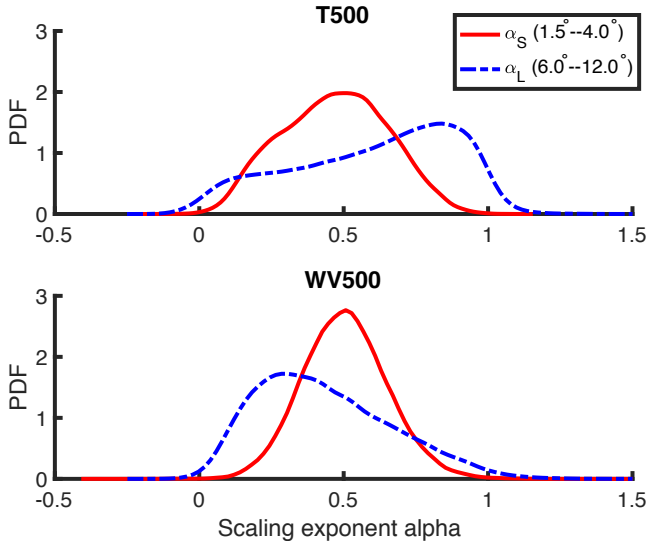

Figure 9. Probability density functions of AIRS-AMSUv6 (top panel) temperature 500 hPa and (bottom panel) water vapor 500 hPa scaling exponents α_L (6.0° - 12°) and α_S (1.5° - 4.0°) derived from five days of observations.

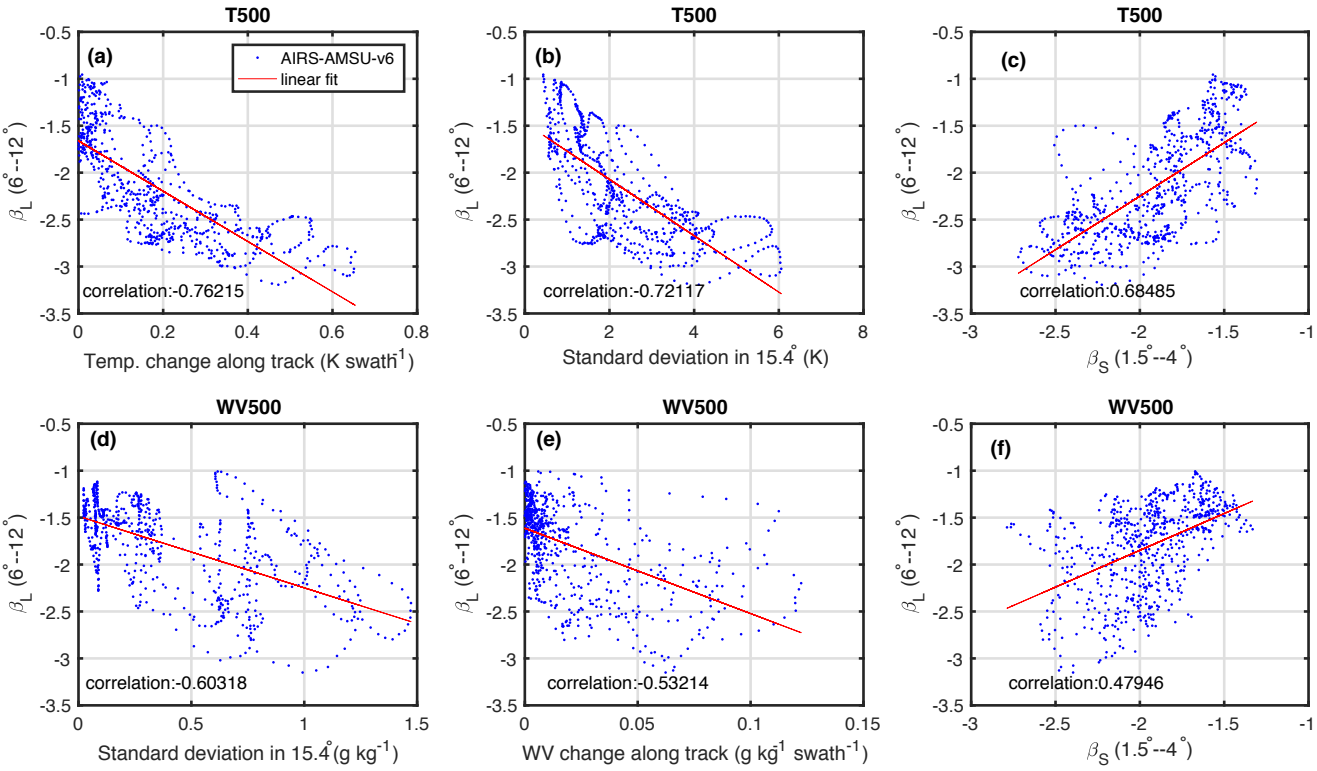

Figure 10. Scatterplots, linear fits and correlations between physical quantities and the slope β_L derived using AIRS-AMSU temperatures at 500 hPa (T500) or water vapor at 500 hPa (WV500) along a 96 min segment of the Aqua track. Panels are ordered from strong (a) to weak (f) correlations.

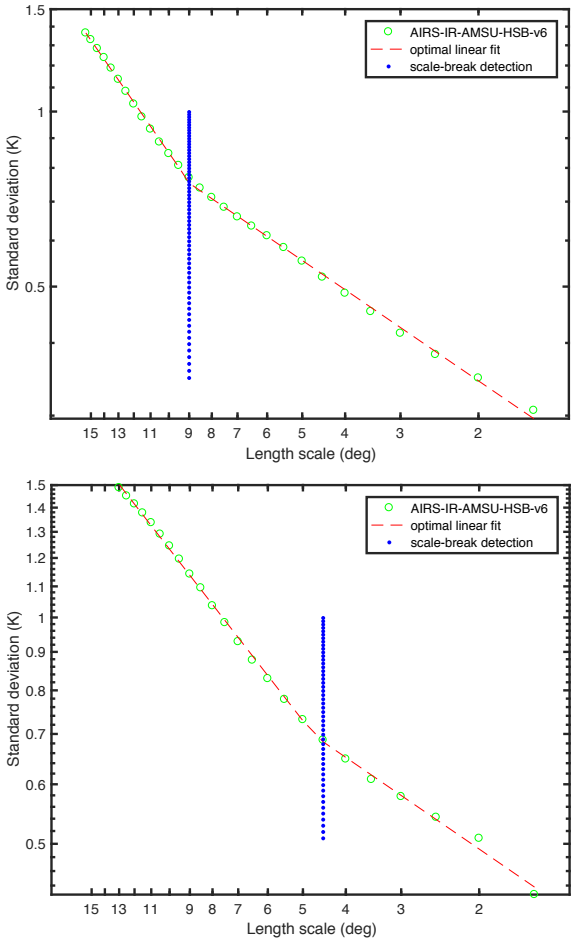

Figure 11. Two variance-scaling plots for AIRS-AMSU-HSB derived temperature at 500 hPa with detected scale breaks: (top panel) North Pacific Ocean (40.3N,141.5W) (bottom panel) North Pacific Ocean (44.6N,142.9W). In the top panel the slope changes at 9° and in the bottom panel at 4.5°.

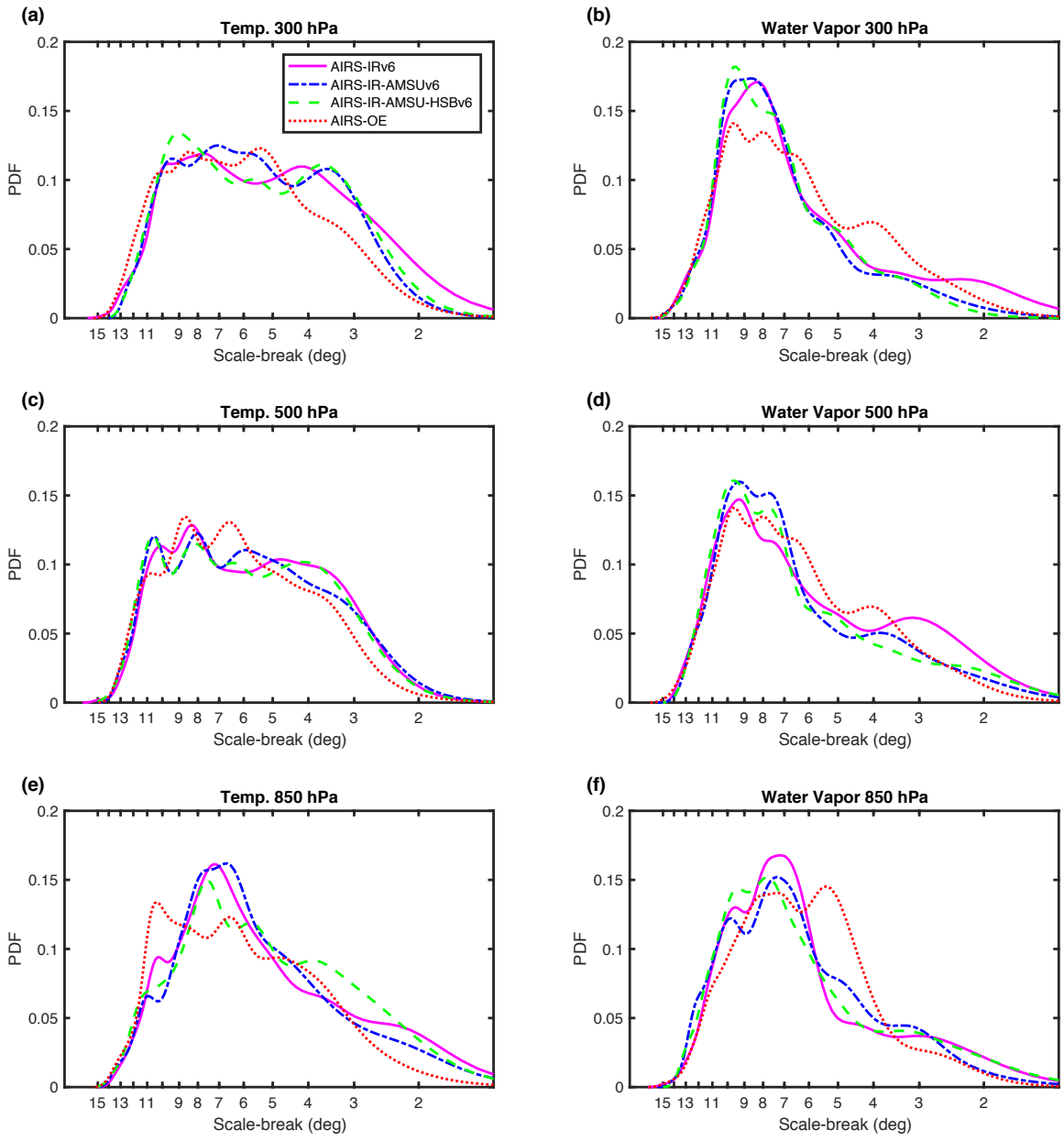

Figure 12. Probability density functions of the scale-break length scale using (left) temperature and (right) water vapor fields at three pressure levels.

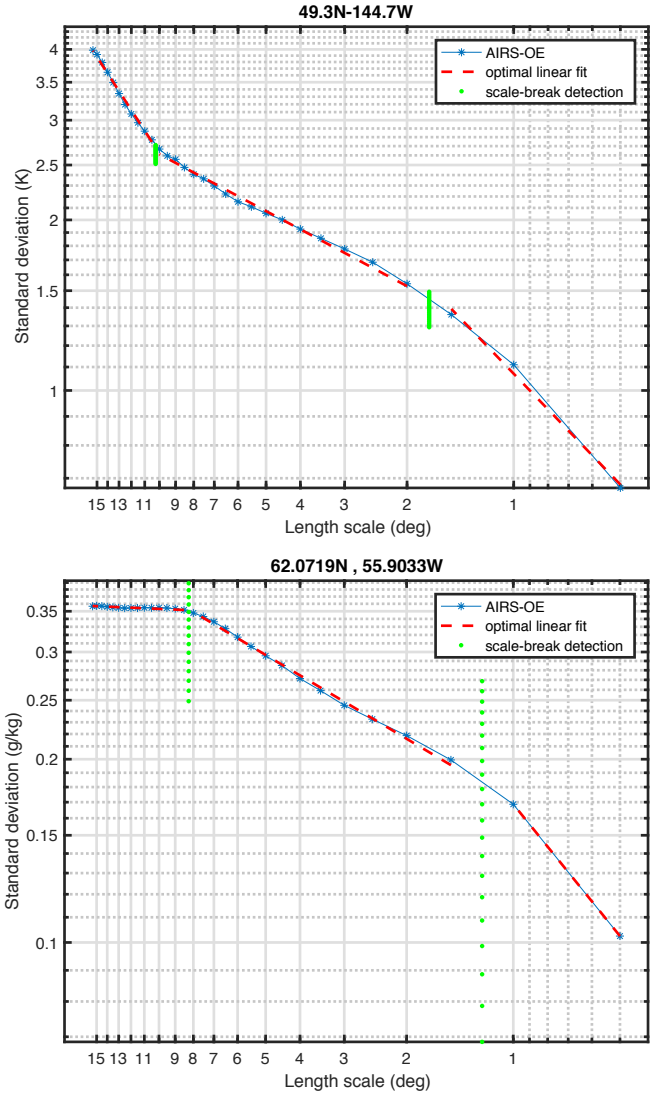

Figure 13. In these double-scale-break examples it can be seen that the slope can change at scales below 1.5°. The standard deviations are calculated with AIRS-OE derived (top) temperature and (bottom) water vapor mass mixing ratio at 500 hPa.